

Chapter 2

Population Balance Models for Pharmaceutical Processes

Anwasha Chaudhury, Maitraye Sen, Dana Barrasso,
and Rohit Ramachandran

Abstract

The pharmaceutical industry is predominantly dominated by the handling of particulate matter in the form of solids and emulsions. With the enforcement of the Quality by Design (QbD) initiative by the Food and Drug Association (FDA), a process systems engineering based case toward particulate process design is advantageous. This suggests the need for mechanistic modeling approaches that can be used for an accurate representation of the process dynamics. The inherent discrete nature of population balance models (PBM) makes it an appropriate framework for modeling particulate processes. With the representation of the particulate processes used for pharmaceutical product manufacturing using various modeling frameworks, advancements can be made to improved control and optimization of the process. This chapter provides a detailed review on the applicability and significance of PBMs in drug product manufacturing and is aimed to provide greater insight into the field of process systems engineering.

Key words Pharmaceutical manufacturing, Population balance model, Flowsheet modeling, Particulate processes, Quality by Design, Process systems engineering

1 Introduction

Particulate processes are ubiquitous in various fields of engineering. Such processes, which are essentially multiphase in nature, are crucial and extensively used in industries, such as pharmaceuticals, detergent manufacturing, polymer processing, and food processing. Within the pharmaceutical industry, these unit operations involve handling of powder or emulsions and transforming their inherent attributes, improving flowability, uniformity, modifying their bioavailability/dissolution characteristics or changing the polymorphic form. Historically, manufacturing costs contributed little to the overall cost of bringing a product to the market. However, due to rising research and development expenditures, rising manufacturing costs, expiration of drug patents, and competition from generic manufacturers, the industry has recognized the need to alter its manufacturing practices to improve operational

efficiency. The proper regulation of such particulate processes in the pharmaceutical industry is of immense importance due to the imposition of a tight quality criteria [75]. The Quality by Design (QbD) initiative launched by the US FDA suggests that quality should be built into a product based on a thorough understanding of the product and process by which it is developed and manufactured, along with an in-depth knowledge of the risks involved in manufacturing the product and procedures to mitigate those risks. Thus, it is beneficial for a pharmaceutical company to implement a process systems engineering-based approach with heavy focus on modeling in order to attain a sustainable position in the market [31, 75, 89]. A model-based systems approach can play a crucial role in the design, operation, evaluation, and analysis of processes because of its potential to provide better process understanding, leading to a reduction in the time and cost for the operation of the process [31, 39].

Processes involving particulate matter cannot be modeled via the continuum approach (e.g., Navier Stokes/momentum balance equation for fluid) since these systems are discrete in nature and can be described using the population balance modeling (PBM) framework. Size, porosity, and composition are some of the critical properties that characterize the end product obtained from these processes. PBMs can be successfully considered for modeling particulate processes, owing to its discrete nature. PBMs are a class of hyperbolic partial differential equations that represent the mesoscopic framework. They involve classification of the particulate population within a process or a system based on discrete set of classes describing their inherent attributes by tracking the number of particles in each class as they are subjected to rate processes. It can be successfully used to relate macroscopic properties based on the information obtained at the microscale. Figure 1 shows the overall pharmaceutical drug manufacturing process starting from the synthesis of the drug. It can be seen that a number of unit operations within the flowsheet (circled) can be conveniently modeled using PBMs, such as crystallization, granulation, milling, mixing, and coating.

PBMs have been very popular for modeling the unit operations involved in the pharmaceutical industry. Significant progression in the application of PBMs for improved pharmaceutical operation has been observed over the past decade [11, 46, 63]. Several researchers have implemented the PBM framework to model the crystallization process [1, 11]. More detailed discussion is presented in the following sections. Granulation has also been modeled using PBMs, but there still exists a lack of available mechanistic knowledge [80]. Milling is yet another poorly understood process which has been described using PBMs [3, 6]. The mixing process has also recently been studied in detail using PBMs [86]. PBMs have also been used to represent coating in order to control and track the

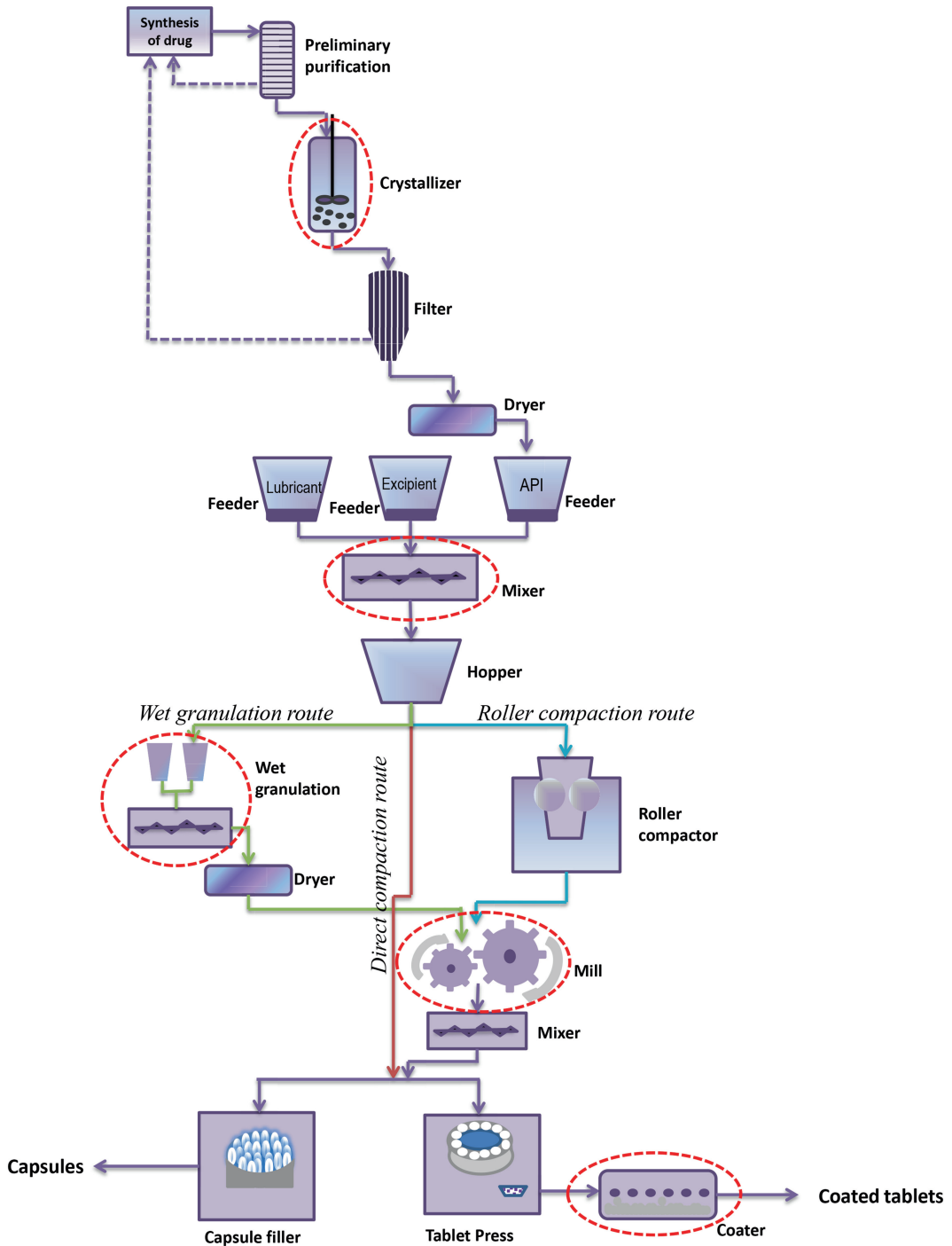


Fig. 1 Schematic of process for continuous drug manufacturing (PBM applicable on the circled unit operations)

coating variability. Coating investigations pertaining to poly-disperse particles are limited in the literature. Experimental observations in a fluid bed coater suggested that coating distribution of the particles is primarily governed by the available surface area [61, 71]. Wnukowski and Setterwall [98] identified two distinct regions within the coater which suggests the existence of an *active zone* (where particles are coated and dried) and the *less active zone* (away from the coating fluid nozzle and near the walls). Later, Maronga and Wnukowski [58] identified three distinct domains within a fluid bed coater suggesting the existence of an *active spray zone*, an *active drying zone* and a *non-active domain*. With this observation, the coating process has been extensively modeled using a compartment based PBM which accounts for the inhomogeneities associated with the existence of distinct regions within the coater [30, 46, 57, 79]. A surface renewal based model has been implemented to model coating processes in order to track the motion of particles between the bulk and spray zone [24, 88]. This approach is useful to identify how particles get replenished in the spray zone with the progress of the operation. Some work has also been performed to model continuous coating processes [42]. However, utilization of PBMs for that purpose has not been explored significantly.

Using a mathematical model that captures the system behavior, various model based control [72] and optimization techniques [32] can be performed which improve the operation of the process. In this article we aim to provide the readers with a detailed discussion on the application of PBMs in modeling particulate processes, followed by solution techniques, implementation of reduced order models in order to combat the high computational overheads associated with solving PBMs and various advanced studies that can be performed using PBMs.

2 Mathematical Model Development

Particulate processes are very common in the pharmaceutical industry although they are very poorly understood due to the lack of mechanistic knowledge in terms of solid handling. The discrete nature of the particulate processes makes it difficult to understand the obscure behavior of such systems. Over the past few decades population balance has been successfully utilized for modeling processes such as crystallization, granulation, coating, milling, and mixing. The PBM in its most general form can be written as [74]:

$$\frac{\partial F}{\partial t}(\mathbf{x}, t) + \frac{\partial}{\partial \mathbf{x}} \left[F \frac{d\mathbf{x}}{dt} \right](\mathbf{x}, t) = b(\mathbf{x}, t, F(\mathbf{x}, t)) \quad (1)$$

where F is the number density of the particulate matter, \mathbf{x} is a vector of internal coordinates whose variation is tracked along the

progression of the process, the partial derivative terms in the left-hand side of the equation represent the growth terms whereas the terms in the right-hand side ($h(x, t, F(x, t))$) depict the source terms involving an overall change in the number of particles. The source terms comprise of the rate of aggregation, breakage, and nucleation. In the following sections further discussion is provided with regard to using PBMs for describing various pharmaceutically relevant processes.

2.1 Crystallization

The crystallization process is used in the initial stages after the synthesis of the drug product. It can be used for various purposes, such as separation, purification, or stabilization of the molecule (through polymorph transformation). This step primarily decides the particle size distribution of the API crystals formed. It is desirable to obtain a uniform size distribution so that the properties of the final pharmaceutical blend remain uniform throughout. Crystallization occurs in two stages. The first stage is nucleation, where several nuclei of a distinct solid phase are formed. The second stage is crystal growth, during which the nuclei grow until a critical crystal size is reached.

When a supersaturated solution is cooled, nucleation and crystal growth takes place, causing the compound concentration in the solution to decrease. Hence, crystallization can be carried out in the manufacturing by manipulating the temperature profile to maintain a specific cooling schedule or by controlling the addition rate of an anti-solvent. When a crystal is formed, it retains some mother liquor that gets occluded within the crystal mass. PBMs are helpful to relate the shape and product size distribution to process parameters.

1-D PBMs have been most commonly used to model crystallization [1, 35, 55], until recently, when some 2-D models have also been developed to describe the crystallization processes [16, 27, 34, 54]. Certain 2-D models also employ the volume and surface area in order to account for the shape of particles [47]. The 1-D and 2-D PBMs are, respectively, shown as

$$\frac{\partial F(L, t)}{\partial t} + \frac{\partial (G(L, C, t)F)}{\partial L} = B_0(C, t)\delta(L) \quad (2)$$

$$\begin{aligned} \frac{\partial F(L_1, L_2, t)}{\partial t} + \frac{\partial (G_1(L_1, L_2, C, t)F)}{\partial L_1} + \frac{\partial (G_2(L_1, L_2, C, t)F)}{\partial L_2} \\ = B_0(C, t)\delta(L_1)\delta(L_2) \end{aligned} \quad (3)$$

Here, the number density, F , is a function of the two length directions and the concentration of solute in the solution. G/G_1 ,

G_2 represent the growth terms in the length direction ($L/L_1, L_2$), and B_0 represents the nucleation term. The growth and the nucleation terms in Eq. (3) can be written as

$$G_1 = k_{g1} \left(\frac{C - C_{sat}}{C_{sat}} \right)^{g_1} \quad (4)$$

$$G_2 = k_{g2} \left(\frac{C - C_{sat}}{C_{sat}} \right)^{g_2} \quad (5)$$

$$B_0 = k_b \left(\frac{C - C_{sat}}{C_{sat}} \right)^b \quad (6)$$

Here, C is the concentration of solute in the solution, C_{sat} is the solubility of the solute at the particular thermodynamic conditions, and k_{g1} , k_{g2} , k_b , g_1 , g_2 , b are the various empirical parameters used to represent growth and nucleation in the form of power law expressions.

Some works have also been observed that consider mother liquor occlusion into the crystal by representing it using a separate dimension [84, 87]. An empirical expression has been obtained for the growth with respect to the additional liquid dimension in order to address the occlusion of liquid into the crystals. From the works of Miki et al. [60], the calculations for mother liquor inclusion in a KDP crystal has been adopted, which was then used to extend the dimensionality of the PBM. Figure 6 in the work of Miki et al. [60] shows the relation between the amount of mother liquor included in the crystal and the size of the crystal. Although the size coordinate considered in the paper was unidimensional, Sen et al. [84] considered two length dimensions. An averaged equivalent length was utilized, which was obtained by calculating the diameter of a sphere with an equal amount of volume as the cuboidal crystal in case of the latter. Considering the depth of the crystal to be L_1 , the equivalent length of the crystal can be expressed as

$$L_{eq}(L_1, L_2) = \left(\frac{6}{\pi} \times L_1^2 L_2 \right)^{\frac{1}{3}} \quad (7)$$

From Eqs. (2) and (3), it can be seen that the number density of particles is a function of the solute concentration, thus indicating the need for a mass balance equation to update the solute concentration in the solution over time. The mass balance equation can be written as

$$\frac{dC}{dt} = -\rho_c \int_0^\infty \int_0^\infty F(L_1, L_2, t) \left(2G_1(L_1 L_2 - L_1^2) + G_2 L_1^2 \right) dL_1 dL_2 \quad (8)$$

where ρ_c is the density of the crystal. The solubility of the solute in the solution is also a function of the temperature of the crystals. Hence, an energy balance equation is also necessary to quantify the change in the temperature, T over time. Aggregation of crystals has also been addressed in several works involving 1-D PBMs [7, 22, 43], however addressing aggregation in the case of multi-dimensional models (while preserving the shape) has not yet been explored. This is primarily due to the lack of mechanistic or statistical information suggesting the propensity of agglomeration based on the length/surface area of the colliding surfaces/length scales. Recently, PBMs have also been employed to study the continuous crystallization process by various researchers [70].

One of the most significant purposes of developing sophisticated models for crystallization processes is the ability to adopt the QbD approach. Using the detailed PBM, the outcome of a crystallization process can be predicted. The crystallization PBM can be calibrated using standard optimization techniques in order to be utilized for predictive purposes. In the work by Sen et al. [85], a 2-D PBM has been employed to validate the model against experimental results. A 2-D PBM enables the crystal shape to be tracked over time and provides more information regarding the progression of the crystallization process. The objective function for the parameter estimation is the minimization of the sum of squared error between the experimental and model predicted concentration. This objective function has been formulated as shown in Eq. (9):

$$\Omega^{\text{Concentration}}(\mathbf{p}) = \sum_{i=1}^n \|C_{\text{predicted}}(t_i, \mathbf{p}) - C_{\text{experimental}}(t_i)\|^2 \quad (9)$$

where Ω represents the objective function, $C_{\text{predicted}}$ and $C_{\text{experimental}}$ represent the predicted and the experimental concentrations, respectively, t_i represents the i th time instant, and \mathbf{p} represents the set of empirical parameters within the PBM.

The shape of the crystal is tracked using the aspect ratio as expressed in Eq. (10):

$$AR(t) = \frac{\sum_{L_1=0}^{L_1 \max} \sum_{L_2=0}^{L_2 \max} F(L_1, L_2, t) \frac{L_1}{L_2}}{\sum_{L_1=0}^{L_1 \max} \sum_{L_2=0}^{L_2 \max} F(L_1, L_2, t)} \quad (10)$$

The optimization was solved using the *fminsearch* function in MATLAB which employs the Nelder–Mead algorithm. Figure 2 presents the validation results using a proprietary molecule. The model reveals good agreement with the experimental

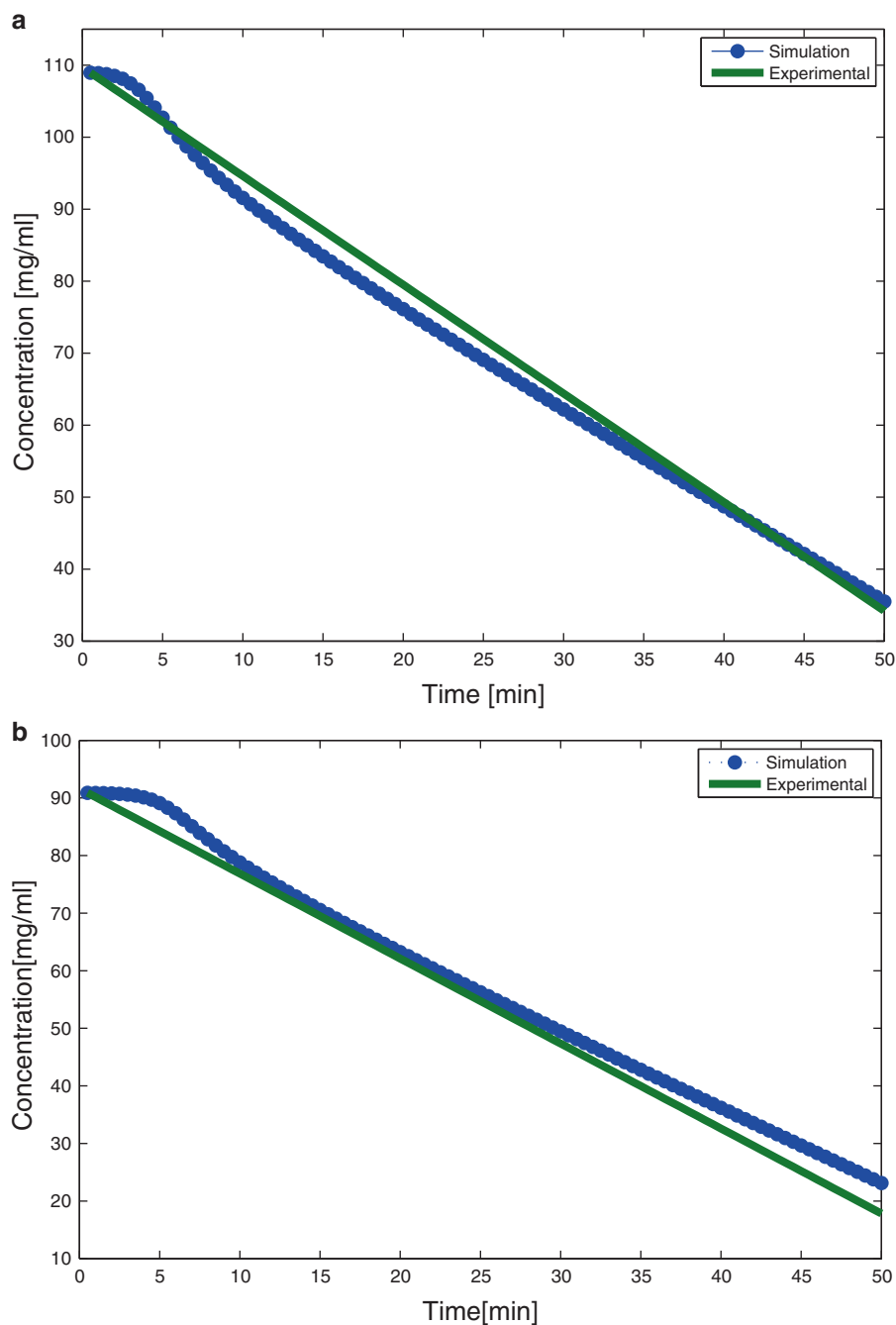


Fig. 2 Validation results from parameter estimation for the evolution of concentration with time for different cooling profiles

observations. The concentration of the solute was fitted with the simulated results using experimental data. The validation results show good agreement between the PBM and the experimental results. Typically, the crystallization process can be calibrated using experimental data consisting of crystal size and shape, the concentration of solute in the mother liquor, temperature or supersaturation of the system. For more advanced studies, other quantities such as polymorph composition or the mother liquor occlusion volume can also be considered.

2.2 Mixing

Mixing is one of the most important unit operations in the downstream tablet manufacturing process. In the pharmaceutical industry, an active pharmaceutical ingredient (API) is mixed with one or more excipients prior to tableting, and the blend quality is primarily determined by the mixing operation. Poor mixing can lead to segregation and result in potency variations in the final dosage form. The outcome of this is a poor quality product which has a higher chance of being out of specification. Mixing is brought about by the particle velocity gradient within the mixer when two or more distinct bulk material particles come into intimate contact. Variability in the mixture is induced by segregation which occurs mainly when particles of different densities tend to settle in different layers [76]. The population balance equation for the mixing process can be written as shown in Eq. (11) [82]. Both internal and external coordinates have been considered, hence a multi-dimensional formulation of the PBM is required.

$$\begin{aligned} \frac{\partial}{\partial t} F(n, x, y, r, t) + \frac{\partial}{\partial x} \left[F(n, x, y, r, t) \frac{dx}{dt} \right] + \frac{\partial}{\partial y} \left[F(n, x, y, r, t) \frac{dy}{dt} \right] \\ + \frac{\partial}{\partial r} \left[F(n, x, y, r, t) \frac{dr}{dt} \right] = \mathfrak{R}_{\text{formation}}(n, x, y, r, t) \\ + \mathfrak{R}_{\text{depletion}}(n, x, y, r, t) + \text{Inflow} - \text{Outflow} \end{aligned} \quad (11)$$

Here, x is the spatial co-ordinate in the axial direction, y is the spatial co-ordinate in the radial direction, and r is the internal co-ordinate of particle size. The counter n stands for the number of components. For example, if the model deals with the mixing of two components (component A and component B), $n = 1$ represents component A and $n = 2$ represents component B. The terms $\frac{dx}{dt}$ and $\frac{dy}{dt}$ represent the velocities in the axial and radial directions, respectively. $F(n, x, y, t)$ is the particle number density (number of particles per unit volume), which varies with the spatial location inside the mixer and the type of particle. Inflow is the rate at which the components are fed to the system, held at a constant value over time. Outflow is the rate at which the components exit the mixer.

Within the pharmaceutical industry, certain API particles are cohesive and tend to stick to each other, forming aggregates. As a result, cohesion leading to aggregation has been studied both experimentally [92] and via DEM simulations [77]. The aggregation rate process is defined in Eqs. (12)–(14):

$$\mathfrak{R}_{\text{aggregation}} = \mathfrak{R}_{\text{formation}} - \mathfrak{R}_{\text{depletion}} \quad (12)$$

where

$$R_{\text{formation}} = 0.5 \int_{r_{\min}}^{r-r_{\min}} \beta(n, x, y, r', r-r') F(n, x, y, r', t) \times F(n, x, y, r-r', t) dr \quad (13)$$

$$R_{\text{depletion}} = \beta(n, x, y, r, r') F(n, x, y, r, t) F(n, x, y, r', t) dr \quad (14)$$

$\beta(n, x, y, r, r')$ is the aggregation kernel defined in Eq. (15). The aggregation kernel is based on the kinetic theory of granular flow (KTGF) [90].

$$\beta(n, x, y, r, r') = K \sqrt{\frac{3\theta}{\rho}} (r + r')^2 \sqrt{\frac{1}{r^3} + \frac{1}{r'^3}} \quad (15)$$

Here K is a constant, ρ is the particle density, and θ is a pseudo-temperature termed granular temperature (Eq. (16)). By definition, v is the random fluctuation of the velocity within a continuous granular medium; however, in this study v is assumed to be the actual particle velocity depicted by its magnitude [33]. This assumption has been deemed valid since the relative differences in the aggregation model are important, as opposed to the absolute differences.

$$\theta = \frac{1}{3} < v \cdot v > \quad (16)$$

In certain cases, formation of aggregates during mixing is not desired. For example, in the pharmaceutical industry, the API is rendered free flowing by addition of suitable lubricants [91]. In the case of free flowing powders, the internal coordinates can be dropped and the population balance equation can be written as shown in Eq. (17):

$$\begin{aligned}
& \frac{\partial}{\partial t} F(n, x, y, t) + \frac{\partial}{\partial x} \left[F(n, x, y, t) \frac{dx}{dt} \right] + \frac{\partial}{\partial y} \left[F(n, x, y, t) \frac{dy}{dt} \right] \\
& = \text{Inflow} - \text{Outflow}
\end{aligned} \tag{17}$$

One of the approaches for modeling a mixer is by dividing it both axially and radially into several compartments. If there are $x_{\max} \times y_{\max}$ compartments, then outflow (as seen in Eq. (11)) can be represented as $\sum_{n=1}^2 \sum_{y=1}^{y_{\max}} F(n, x_{\max}, y, t) V_f$, which is the total number of particles exiting from the end compartments. V_f is the forward axial velocity. Mixing can occur in both the axial and radial directions by convection and dispersion. In a continuous mixer, mixing takes place when the particles are moved about by the motion of the blades with the dispersive component being negligibly small relative to the convective one. Such assumptions have been justified in literature [66]. Particles can be treated as discrete entities and their exchange between any two compartments is simulated. It is assumed that homogeneous mixing occurs in each of the compartments. The axial and radial velocities move the particles from one compartment to another in both the axial and radial directions. The exchange of mass between the compartments has been represented as a number of particles. Particles can either move forward to the compartment ahead of it or backward to the compartment behind it. On the other hand, radial mixing conserves the total number of particles at a fixed axial location at any given point in time. Hence the mass exchange (in terms of particle density) of a single component among the compartments can be simplified according to Eq. (18), given below:

$$\begin{aligned}
\frac{\partial F(n, x, y, t)}{\partial t} = & \frac{V_f [F_{n, x-1, y, t} - F_{n, x, y, t}]}{\Delta x} + \frac{V_b [F_{n, x+1, y, t} - F_{n, x, y, t}]}{\Delta x} \\
& + V_r \frac{[F_{n, x, y+1, t} + F_{n, x, y-1, t} - 2F_{n, x, y, t}]}{\Delta y}
\end{aligned} \tag{18}$$

The above equation can be written for each component present in the mixer. Here, V_f refers to the forward velocity in the axial direction, V_b refers to backward velocity in the axial direction, and V_r refers to the radial velocity.

The inputs to this model are V_f , V_b , and V_r . The velocity values can be obtained either experimentally or from a previously run detailed numerical simulation (e.g., DEM simulation). DEM calculates the velocity values from the particle properties (e.g., particle diameter, density). Once velocity values are extracted, the simulation can be used to provide information about the dynamics and the outputs of the process.

Consider a case where two components (component A and component B) are being mixed, where component A can be taken as the API and component B as the excipient. At inlet, the flowrate of the component A (API) is 16.3 % of the total flowrate (i.e., the sum of component A and component B inlet flowrates). The input parameters V_f , V_b , and V_r have been obtained from a previously run DEM simulation, where a continuous mixer has been simulated using EDEMTM (DEM Solutions). A commercial mixer (Gericke GCM250TM) with impeller blades in alternating forward and backward orientation has been simulated. Equal number of particles each of component A and B have been introduced into the mixer using two feeders discharging particles on either side of the inlet. A feed rate of 1990 particles per second and an impeller speed of 250 RPM have been maintained. The details of the DEM simulation and velocity extraction have been previously reported by the authors [86]. The mixing performance is defined in terms of certain critical quality attributes (CQAs) such as relative standard deviation (RSD), composition of A, which can be active ingredient of interest for a given process (C_A) and residence time distribution (RTD). These CQAs should be regulated and controlled in order to achieve the desired mixing efficiency. These parameters can be found as described below:

$$C_A = \frac{\sum_{y=1}^{y_{\max}} F(1, x_{\max}, y, t)}{\sum_{n=1}^{n_{\max}} \sum_{y=1}^{y_{\max}} F(n, x_{\max}, y, t)} \quad (19)$$

In the above equation, the numerator stands for the total number of particles of component A which exit from the last compartments at any point in time. The denominator represents total number of particles of both components A and B exiting from the last compartments at any point of time. Since this model involves two components, the value of n_{\max} is 2. x_{\max} and y_{\max} stand for the maximum number of grids in the axial and radial directions, respectively. Figure 3 shows how the API composition at the mixer outlet varies over time. It can be seen that the API composition at the outlet increases with time and finally reaches a steady value of 0.163 (which is same as the inlet composition).

The homogeneity of samples retrieved from the outflow is measured by calculating the variability in the concentration. The RSD of the tracer concentration measures the degree of homogeneity of the mixture and is given by

$$RSD = \frac{\sqrt{\sum_{i=1}^N \frac{(c_i - c_{\text{avg}})^2}{N-1}}}{c_{\text{avg}}} \quad (20)$$

where N represents the total number of compartments ($N = x_{\max} \times y_{\max}$). i is the index to represent the compartment. c_i is the

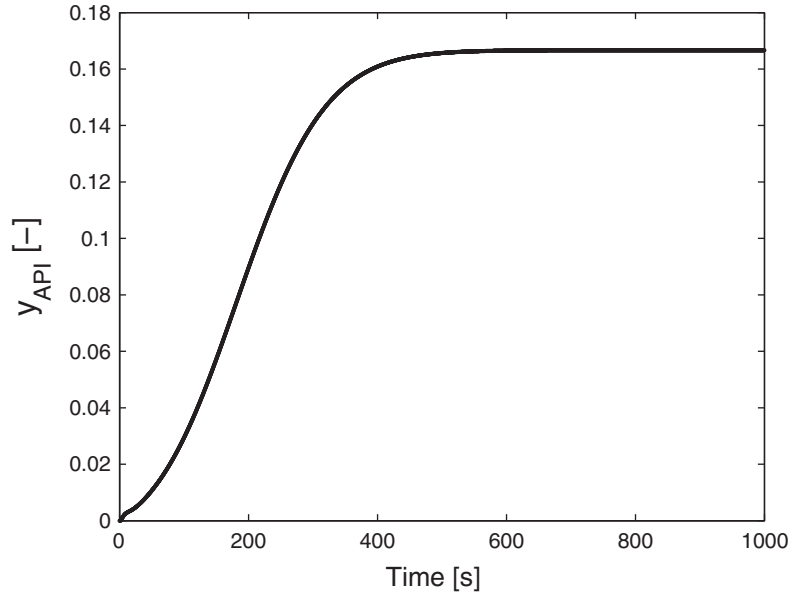


Fig. 3 Evolution of API composition

concentration of component A at any compartment i . c_{avg} is a spatial average of the concentration of component A. Figure 4 represents how the overall RSD decreases over time as well as over the mixer length. This is because the variability in the mixture is reduced over time. In Fig. 4, the mixer length is represented by the compartment number. The spikes present in the graph depict back mixing in the respective compartments.

The RTD, $E(t)$, is a measure of the time spent by the particles within the mixer, capturing the non-ideality associated with the flow. The RTD can be found by

$$E(t) = \frac{c(t)}{\int_0^\infty c(t) dt} \quad (21)$$

In the above equation, $c(t)$ stands for the concentration of component A in the outlet stream at any time t . It is important to make the following assumptions in order to determine the RTD: (1) the flow in the mixer is well mixed; (2) the powder elements entering the mixer simultaneously flow with constant velocity and leave the mixer at same time. Figure 5 depicts the RTD of the API in the mixer upon injecting a pulse of API at $t = 100$ s. The RTD is a measure of the time spent by the API particles in the mixer and correlates to mixing performance. The width of the RTD curve can

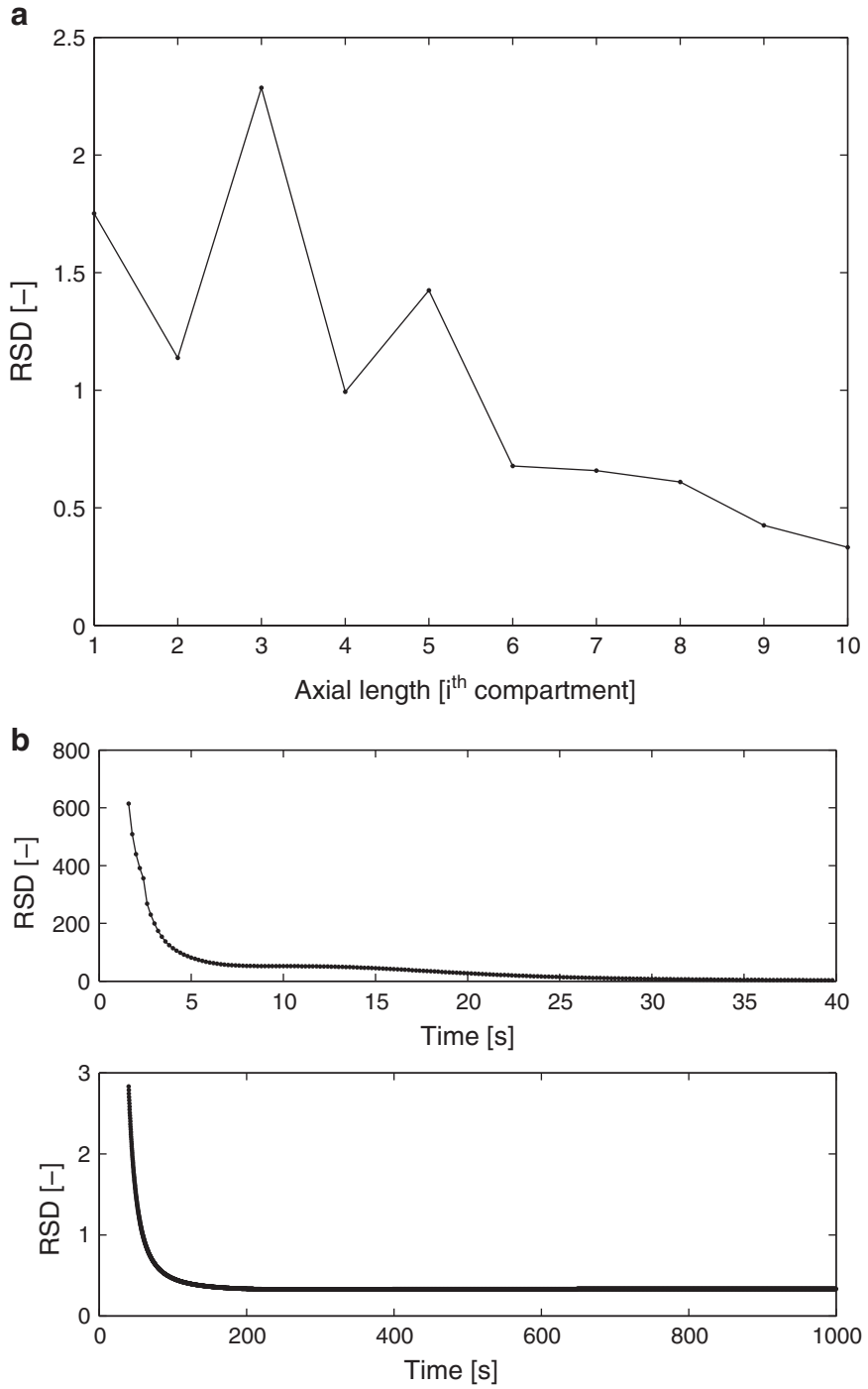


Fig. 4 Plot of (a) RSD versus axial length at end-point and (b) RSD versus time at mixer outlet for 0:40 s and 40:1000 s

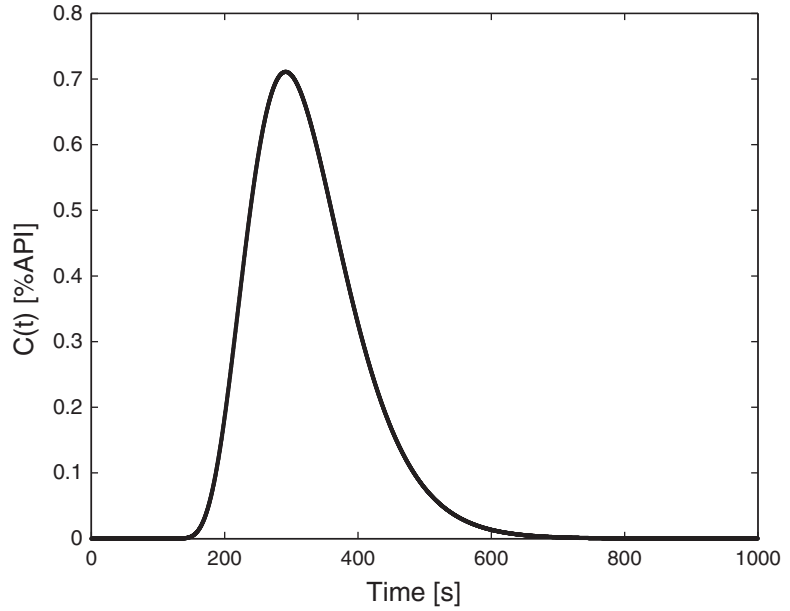


Fig. 5 RTD of API upon injection of pulse at $t = 100$ s

be set as a metric to optimize process performance as a function of formulation properties and processing conditions.

The mathematical model has been validated with experimental results. Experiments have been designed to obtain the RSD and API composition at the mixer outlet as a function of time. Materials, which have been used in the experiment are Avicel PH-200 (FMC biopolymer), which is the excipient and Acetaminophen (Mallinckrodt), which is the API. The mixing has been carried out in a commercial mixer (Gericke GCM250TM). One experimental data set which has been obtained for a feed rate of 20 kg/h and mixer speed of 40 RPM has been considered. API concentration in the mixture fed to the mixer inlet is 10 %. More details on the experimental setup can be obtained from [83]. The API composition and RSD values have been obtained as a function of time at the mixer outlet. A linear trendline has been fitted to the experimental data points and the model has been validated with respect to the trendline. The objective function can be formulated as shown below (Eqs. (22)–(24)) [83]:

$$\Omega^{\text{APIComposition}}(p) = \sum_{i=1}^n \left\| y_{\text{API,predicted}}(t_i, \mathbf{p}) - y_{\text{API,experimental}}(t_i) \right\|^2 \quad (22)$$

$$\Omega^{\text{RSD}}(p) = \sum_{i=1}^n k \left\| \text{RSD}_{\text{predicted}}(t_i, \mathbf{p}) - \text{RSD}_{\text{experimental}}(t_i) \right\|^2 \quad (23)$$

\mathbf{p} is the set of estimated parameters, which, in this case, are the forward, backward, and radial velocities (V_f , V_b , and V_r). The objective function for the RSD has been multiplied by a constant (k) to facilitate convergence since the API composition and RSD have values of different orders. The overall objective function was then formulated as follows:

$$\Omega^{\text{Total}}(p) = \Omega^{\text{RSD}}(p) + \Omega^{\text{APIComposition}}(p) \quad (24)$$

An RTD study has been performed, as well. Since the RTD measurement requires a different set of experiment, the objective function has been formulated and optimized separately, as shown in Eq. (25):

$$\Omega^{\text{RTD}}(p) = \sum_{i=1}^n \|E_{\text{predicted}}(t_i, \mathbf{p}) - E_{\text{experimental}}(t_i)\|^2 \quad (25)$$

Figure 6 shows that there is a good agreement between the model predicted and experimental (linear trendline) values for both RSD and API composition.

2.3 Granulation

Granulation is yet another crucial process that is very relevant to the pharmaceutical industry. It involves the size enlargement of particles in order to improve flowability and dissolution and enhance homogeneity of finer particulate solids. It is a highly complex process that is poorly understood and is currently operated in the industry under high recycles [80]. Due to the discrete nature of the process, PBMs are highly useful in modeling granulation [48]. In early days, 1-D models were more popular for modeling granulation due to their reduced complexity [53, 81]. However, Iveson [38] presented a detailed case study emphasizing the need for multi-dimensional models for accurately modeling granulation. Eventually, Wauters [97] suggested an easier yet effective approach of framing a multi-dimensional population balance model for granulation by re-casting it in terms of their individual volumes of solid (s), liquid (l), and gas (g), which enables the decoupling of the integrated process with respect to the individual meso-scopic sub-processes. The overall 3-D PBM for granulation can be written as

$$\begin{aligned} \frac{\partial}{\partial t} F(s, l, g, t) + \frac{\partial}{\partial s} \left[F(s, l, g, t) \frac{ds}{dt} \right] + \frac{\partial}{\partial l} \left[F(s, l, g, t) \frac{dl}{dt} \right] \\ + \frac{\partial}{\partial g} \left[F(s, l, g, t) \frac{dg}{dt} \right] = \mathfrak{R}_{\text{nuc}} + \mathfrak{R}_{\text{agg}} + \mathfrak{R}_{\text{break}} \end{aligned} \quad (26)$$

where $F(s, l, g, t)$ represents the population density function such that $F(s, l, g, t)dsdl dg$ is the number of moles of granules with a

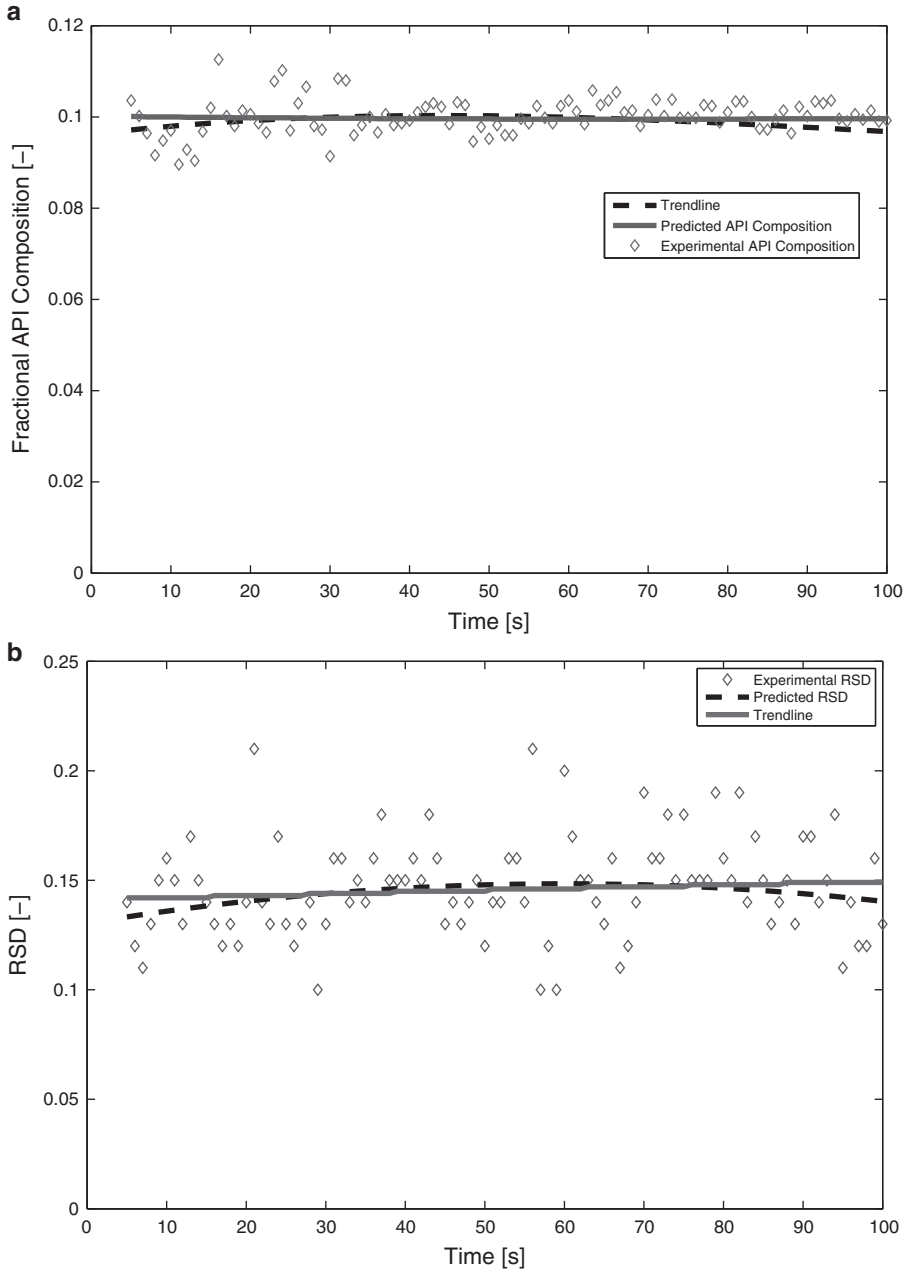


Fig. 6 (a) Fractional API composition versus time at mixer outlet and (b) RSD versus time at mixer outlet

solid volume between s and $s + ds$, a liquid volume between l and $l + dl$, and a gas volume between g and $g + dg$. The partial derivative term with respect to s accounts for the layering of fines onto the granule surfaces, the partial derivative term with respect to l accounts for the drying of the binder or the re-wetting of granules and the partial derivative with respect to g accounts for

consolidation, which, due to compaction of the granules, results in an increase in the pore saturation and decrease in the porosity.

Various submodels can be used to describe the different growth mechanisms involved in granulation. Wang et al. [96] modeled the layering of fines using a Monod based growth model as shown in Eq. (27):

$$G = G_{\max} \frac{M_{\text{powder}}}{k_i \sum M_i + M_{\text{powder}}} e^{[-\alpha(x_w - x_{wc})^2]} \quad (27)$$

where G_{\max} is the maximum growth rate, M_{powder} is the mass of fine powder, M_i is the mass of particles in the i th size class, x_{wc} is the critical moisture, and k and α are fitting parameters (based on experimental data-particle size distribution, porosity, moisture content). Layering is highly affected by the amount of fines present in the system.

Drying and rewetting are associated with the gain or loss of liquid into or from the granulation system due to evaporation or liquid addition. The liquid growth rate can be obtained from the mass balance as

$$\frac{dL}{dt} = \frac{\dot{m}_{\text{spray}}(1 - c_{\text{binder}}) - \dot{m}_{\text{evap}}}{m_{\text{solid}}}, \quad (28)$$

where

$$m_{\text{solid}} = m_{\text{solid fraction}} + \dot{m}_{\text{spray}} c_{\text{binder}} \Delta t, \quad (29)$$

In the above equations, \dot{m}_{spray} is the rate at which liquid is being sprayed in the system, c_{binder} is the concentration of solid binder in the liquid added, \dot{m}_{evap} is the rate of liquid being evaporated, $m_{\text{solid fraction}}$ is the volume of solid of the particles in each bin and L is the liquid in the powder bed. In the case of a high shear mixer, the assumption of $\dot{m}_{\text{evap}} = 0$ is valid. However, in the case of a fluid bed process, the evaporation rate dominates over rewetting, and thus the evaporation term needs to be taken into account [18].

Consolidation is a negative growth process which represents the compacting of granules due to the escape of air from the pores. It can be modeled as an empirical exponential decay relation [94], given by

$$\frac{d\varepsilon}{dt} = -c(\varepsilon - \varepsilon_{\min}), \quad (30)$$

$$\frac{dg}{dt} = \frac{c(s + l + g)(1 - \varepsilon_{\min})}{s} \times \left[l - \frac{\varepsilon_{\min}s}{1 - \varepsilon_{\min}} + g \right] \quad (31)$$

where the porosity ε is

$$\varepsilon = \frac{l + g}{s + l + g} \quad (32)$$

Here ε_{\min} is the minimum porosity of the granules and c is the compaction rate constant.

The above equations adequately represent the growth terms that are observed on the left side of the PBM (Eq. (26)). The source terms on the right side of Eq. (26) comprise of nucleation, agglomeration, and breakage. Aggregation of particles is one of the dominant mechanisms that enables size enlargement during granulation. The aggregation of particles is obtained as a combination of the formation and depletion terms as shown in Eqs. (34) and (35):

$$\mathfrak{R}_{\text{agg}}(s, l, g) = \mathfrak{R}_{\text{agg}}^{\text{form}} - \mathfrak{R}_{\text{agg}}^{\text{dep}} \quad (33)$$

such that

$$\begin{aligned} \mathfrak{R}_{\text{agg}}^{\text{form}} = & \frac{1}{2} \int_{s_{\min}}^{s_{\max}} \int_0^{l_{\max}} \int_0^{g_{\max}} \beta(s', s - s', l', l - l', g', g - g') \\ & \times F(s', l', g', t) F(s - s', l - l', g - g', t) ds' dl' dg' \end{aligned} \quad (34)$$

$$\begin{aligned} \mathfrak{R}_{\text{agg}}^{\text{dep}} = & F(s, l, g, t) \int_{s_{\min}}^{s_{\max}} \int_0^{l_{\max}} \int_0^{g_{\max}} \beta(s', s - s', l', l - l', g', g - g') \\ & \times F(s', l', g', t) ds' dl' dg' \end{aligned} \quad (35)$$

where s_{\min} is the minimum solid volume of the particles present in the system and $\beta(s', s - s', l', l - l', g', g - g')$ is the size-dependent aggregation kernel that describes rate expression for aggregation of two granules of internal coordinates (s', l', g') and $(s - s', l - l', g - g')$. The formation term accounts for the new particles that are formed after coalescence, whereas the depletion term accounts for the particles that are lost when the smaller particles coalesce and aggregate. The PBM has been validated against experimental data by calibrating the model using parameter estimation techniques. Figure 7 shows agreement between the experimental and predicted results for the mean diameter and porosity of the product class for the granules. It can be seen that the model is able to

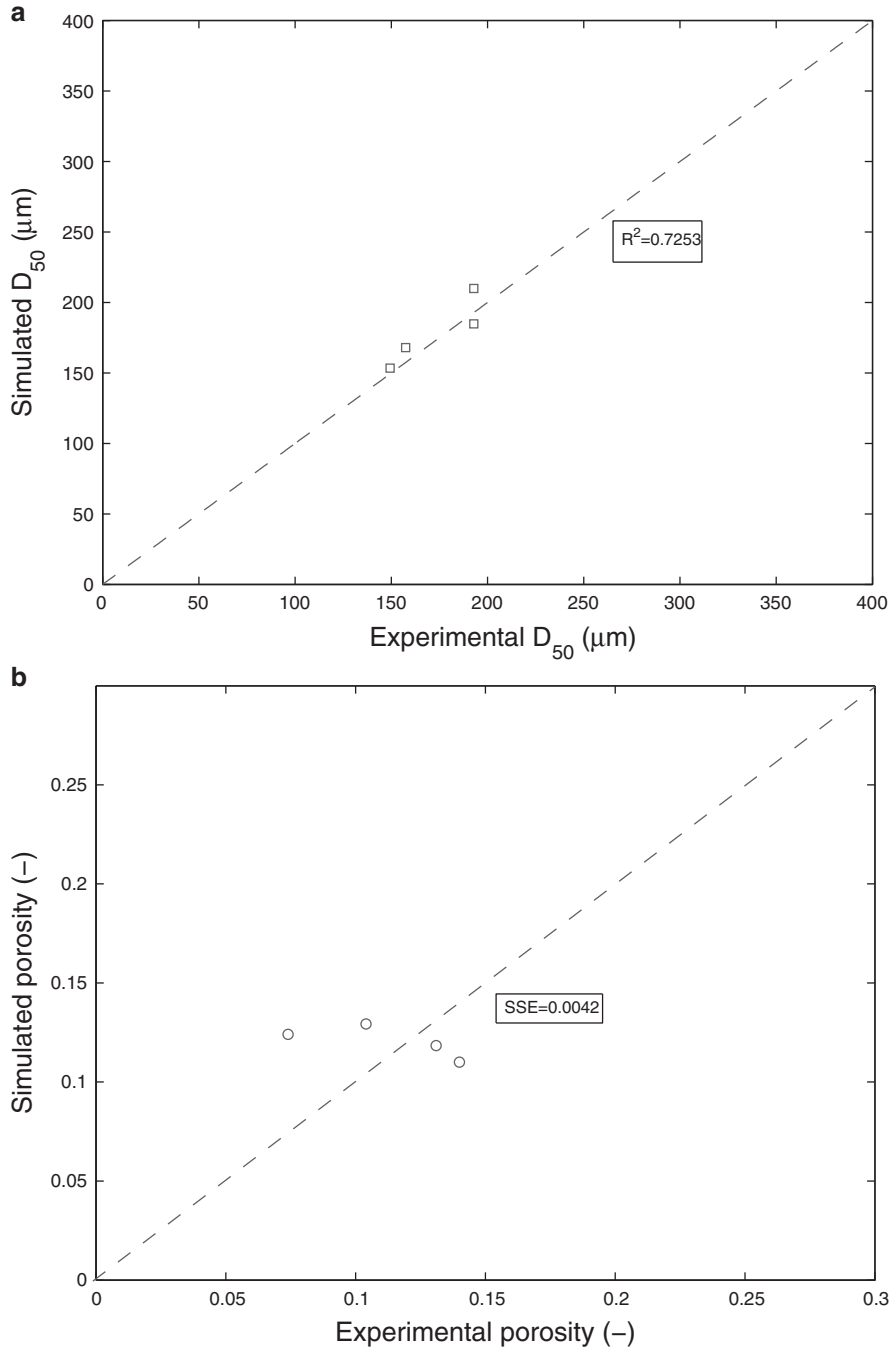
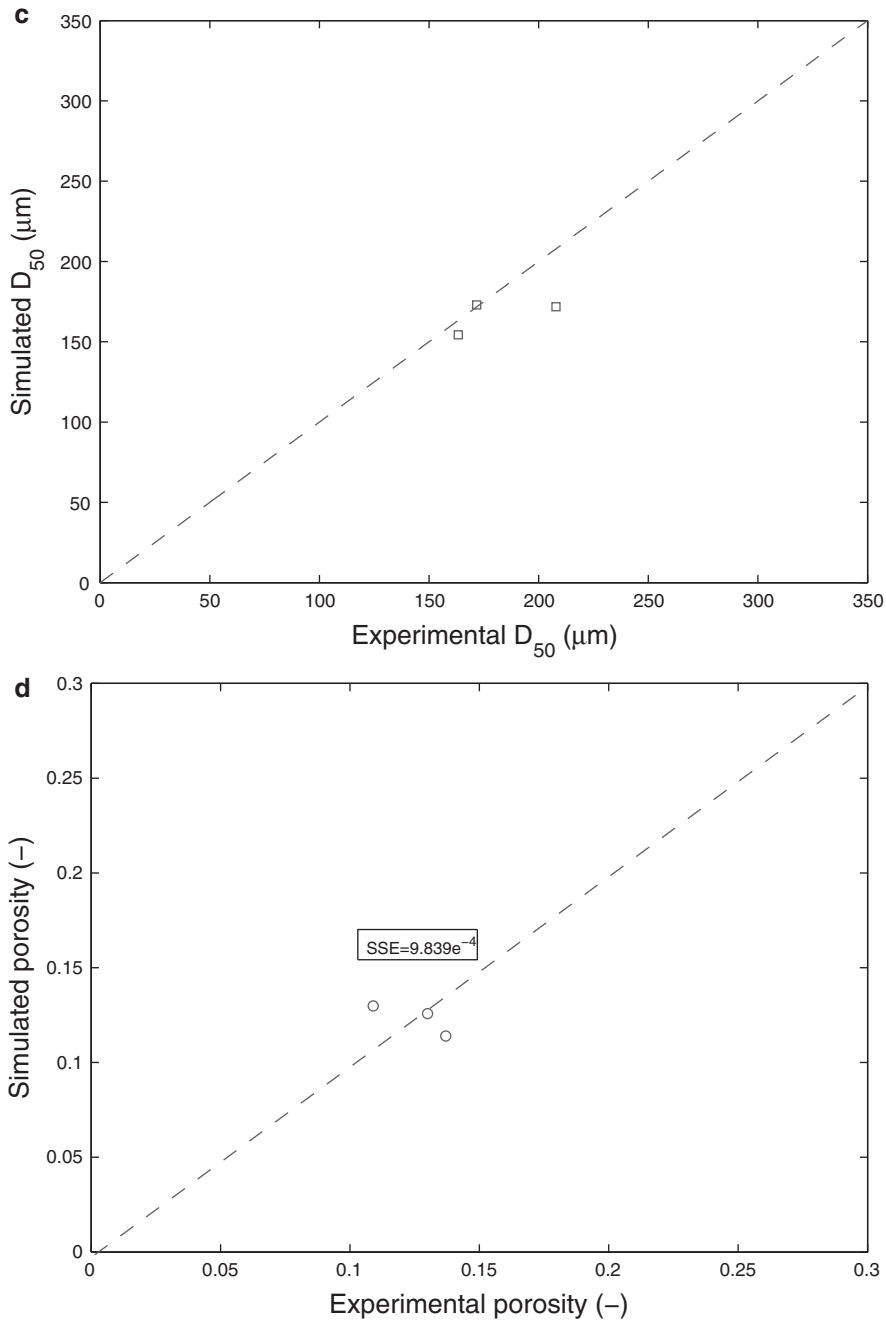


Fig. 7 Estimations and predictions for a high shear granulator using PBM. (a) Experimental and estimated simulated D_{50} , (b) experimental and estimated simulated porosity, (c) experimental and predicted D_{50} , and (d) experimental and predicted porosity

**Fig. 7** (continued)

capture the experimental trends and also make close predictions. The 45° dotted line depicts the condition where the simulated values equal the experimental results (perfect agreement). The proximity of the points to the dotted 45° line shows the accuracy in the approximation. This suggests the applicability towards QbD for improved process operation.

The appropriate selection of the aggregation kernel is also a crucial task in accurate modeling of a granulating system. Many empirical kernels have been observed in literature, but a mechanistic kernel is most desirable as it takes into account the various material and system properties and can hence be extrapolated for different systems. An empirical kernel requires more number of parameters that have to be tuned in order to tailor the kernel to a particular system. This makes an empirical kernel extremely system specific and thus cannot be generalized. A list of the various aggregation kernels available in literature has been shown in a tabular form by Cameron et al. [12]. The approach based on [26] and [50, 51] was implemented by Immanuel and Doyle [37] in order to obtain a mechanistic kernel, which takes into account various system parameters, such as particle diameter and temperature, resulting in a more generalized kernel which requires fewer estimated parameters. A modified physical-based kernel has also been proposed recently, which considers variable binder thickness for obtaining the aggregation kernel [52]. A novel semi-mechanistic kernel has been recently proposed that takes into account the influence of various measurable operating parameters on the final granule properties and yet is computationally inexpensive [21]. This model can effectively capture the steady and induction growth behaviors that have been observed experimentally. Figure 8 depicts the ability of the semi-mechanistic kernel to be able to capture the various growth behaviors. For highly porous starting particles, the growth in particle size is not observed immediately after the onset of liquid addition. Growth is brought about only after there is sufficient consolidation to squeeze out liquid which can then aid with agglomeration. Therefore, there is a delay with the growth of particle size. This scenario is called induction growth. The granulation of less porous particles, however, starts immediately after the addition of liquid. This is known as steady growth. Figure 8 not only captures the influence of crucial operating parameters, e.g. viscosity (higher viscosity suggests higher viscous forces thus forming bigger granules), but is also able to demarcate the existence of induction vs steady growth. As expected intuitively, the growth of primary particles is aided on increasing the viscosity of the binder. The highly viscous binder is more efficient with dissipating the kinetic energy through viscous forces.

Breakage is the disintegration of a particle into two or more fragments and is mainly governed by attrition and impact. It plays a crucial role in controlling the final granule size distribution in high shear granulators. Many published breakage kernels have been presented in literature, one of which defines the breakage kernel in terms of empirical parameters and shear rate [64]. Mechanistic kernels have also been proposed in literature, where the kernel has

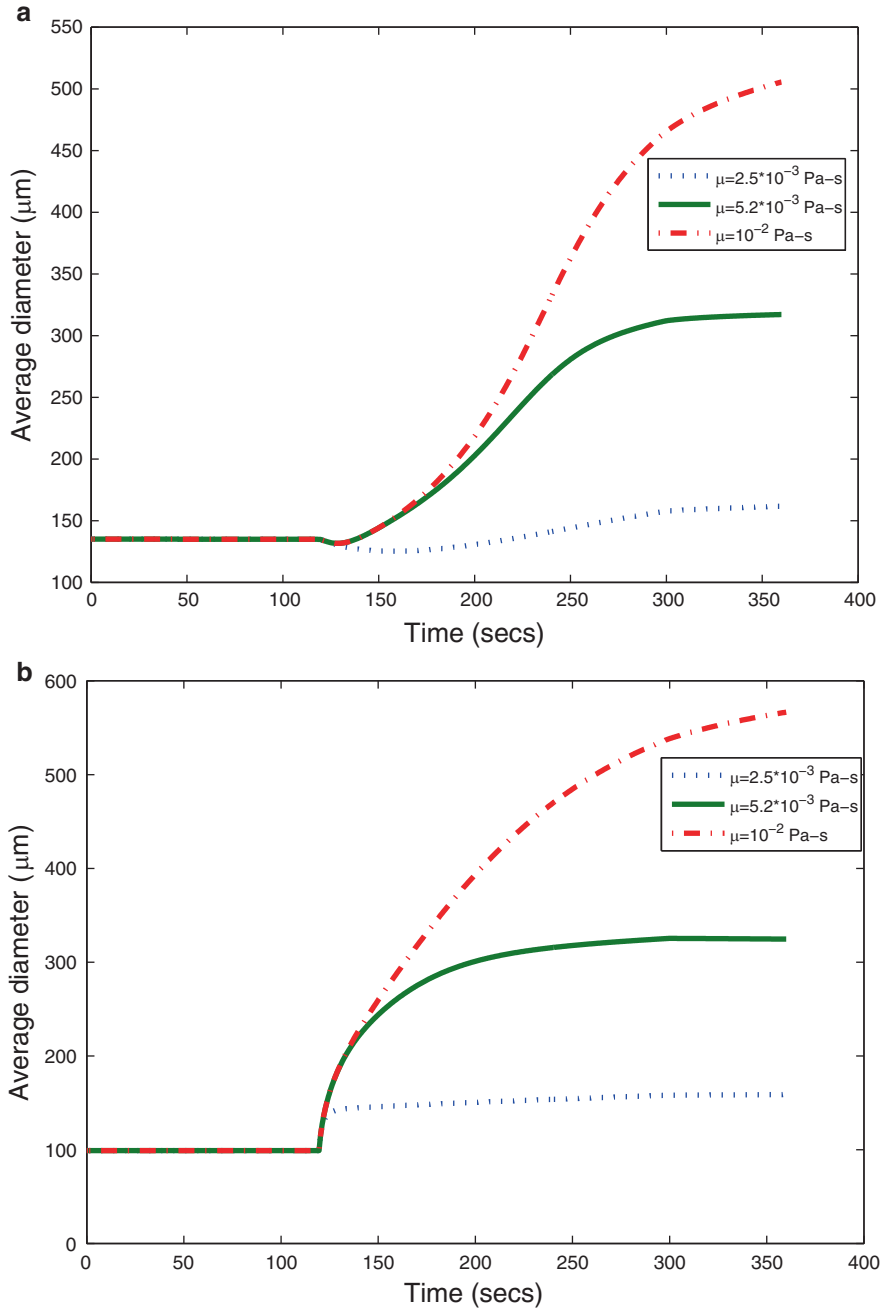


Fig. 8 Effect of viscosity from model results revealing steady and induction growth behavior for low and high porous particles respectively. (a) Induction growth for highly porous particles and (b) steady growth for less porous particles

been expressed to be proportional to the ratio of the external stress to the intrinsic strength [73].

Several models have been developed in order to quantify the breakage distribution function [65]. Using this information, the breakage term can be broken into its corresponding birth and death terms as

$$\mathfrak{R}_{\text{break}}(s, l, g) = \mathfrak{R}_{\text{break}}^{\text{form}} - \mathfrak{R}_{\text{break}}^{\text{dep}}, \quad (36)$$

such that the birth and death terms can be explained using Eqs. (37) and (38):

$$\begin{aligned} \mathfrak{R}_{\text{break}}^{\text{form}} &= \int_0^{s_{\max}} \int_0^{l_{\max}} \int_0^{g_{\max}} K_{\text{break}}(s, l, g) b(s', s - s', l', l - l', g', g - g') \\ &\quad \times F(s', l', g', t) ds' dl' dg' \end{aligned} \quad (37)$$

$$\mathfrak{R}_{\text{break}}^{\text{dep}} = K_{\text{break}}(s, l, g) F(s, l, g, t). \quad (38)$$

A more mechanistic approach towards obtaining the breakage kernel has also been proposed by Ramachandran et al. [73] where the K_{break} has been represented as a ratio of the external stress to the internal stress. These stresses have been further obtained by applying the physics of the system combined with the information of the various microscopic properties. Breakage has also been studied using a non-linear effect on the mechanism for milling processes by Bilgili and Scarlett [6].

The effect of the various underlying mechanisms governing granulation has been presented in [15]. The effect of the primary particles and the binder addition mode has also been studied.

A continuous granulation operation has also been studied recently in the work by Barrasso et al. [4]. The continuous granulator has been subdivided into three distinct zones demarcating the premixing zone, the spray zone, and the wet massing zone. The multidimensional PBM for the continuous process is expressed as a function of the internal and the external coordinates in order to address the inhomogeneities based on the spatial positions (as shown in Eq. (39)):

$$\begin{aligned}
& \frac{\partial}{\partial t} F(s_1, s_2, l, g, x, y, t) + \frac{\partial}{\partial s_1} \left[F(s_1, s_2, l, g, x, y, t) \frac{ds_1}{dt} \right] \\
& + \frac{\partial}{\partial s_2} \left[F(s_1, s_2, l, g, x, y, t) \frac{ds_2}{dt} \right] + \frac{\partial}{\partial l} \left[F(s_1, s_2, l, g, x, y, t) \frac{dl}{dt} \right] \\
& + \frac{\partial}{\partial g} \left[F(s_1, s_2, l, g, x, y, t) \frac{dg}{dt} \right] \frac{\partial}{\partial x} \left[F(s_1, s_2, l, g, x, y, t) \frac{dx}{dt} \right] \\
& + \frac{\partial}{\partial y} \left[F(s_1, s_2, l, g, x, y, t) \frac{dy}{dt} \right] \\
& = \dot{F}_{\text{in}}(s_1, s_2, l, g, x, y, t) + \dot{F}_{\text{out}}(s_1, s_2, l, g, x, y, t) \\
& + \mathfrak{R}_{\text{nuc}} + \mathfrak{R}_{\text{agg}} + \mathfrak{R}_{\text{break}}
\end{aligned} \tag{39}$$

The modeling results could very well capture the experimental trends that were observed in practice (see Fig. 9). A detailed parametric study involving the study of the various crucial operating parameters has also been studied [4]. Findings suggest that the residence time and liquid-to-solid ratio are the most critical parameters in determining the product size distribution in twin screw granulation. The residence time is the result of design parameters, such as screw length and configuration, as well as process parameters, such as screw speed and throughput. The model calibration for the granulation process requires experimental data consisting of the particle size distribution and porosity in typical cases. The tight quality criteria in the pharmaceutical industry requires the particle size to lie within a certain range, such that the dissolution and bioavailability of the drug can be controlled. The granule size can be measured using various equipments measuring the size or using the sieve analysis. Sieve analysis is a more crude method and is generally associated with a relatively high measurement error [63].

2.4 Milling

Milling is a particle size reduction process often used in pharmaceutical manufacturing of solid oral dosage forms. Used for delumping in the direct compaction manufacturing route, milling processes have additional purposes in wet and dry granulation manufacturing routes. In dry granulation, a roller compactor is used to form compacted ribbons from fine powder. Milling is then used to produce granules from these ribbons. In manufacturing routes using wet granulation, milling operations can be used to reduce oversize particles following granulation and increase amount of the product within the desired size class.

The conical screen mill, which is most widely used for pharmaceutical applications, applies strong shear forces on particles that are trapped between the impeller and the screen, resulting in particle attrition [3]. Small fragment particles are able to pass through the

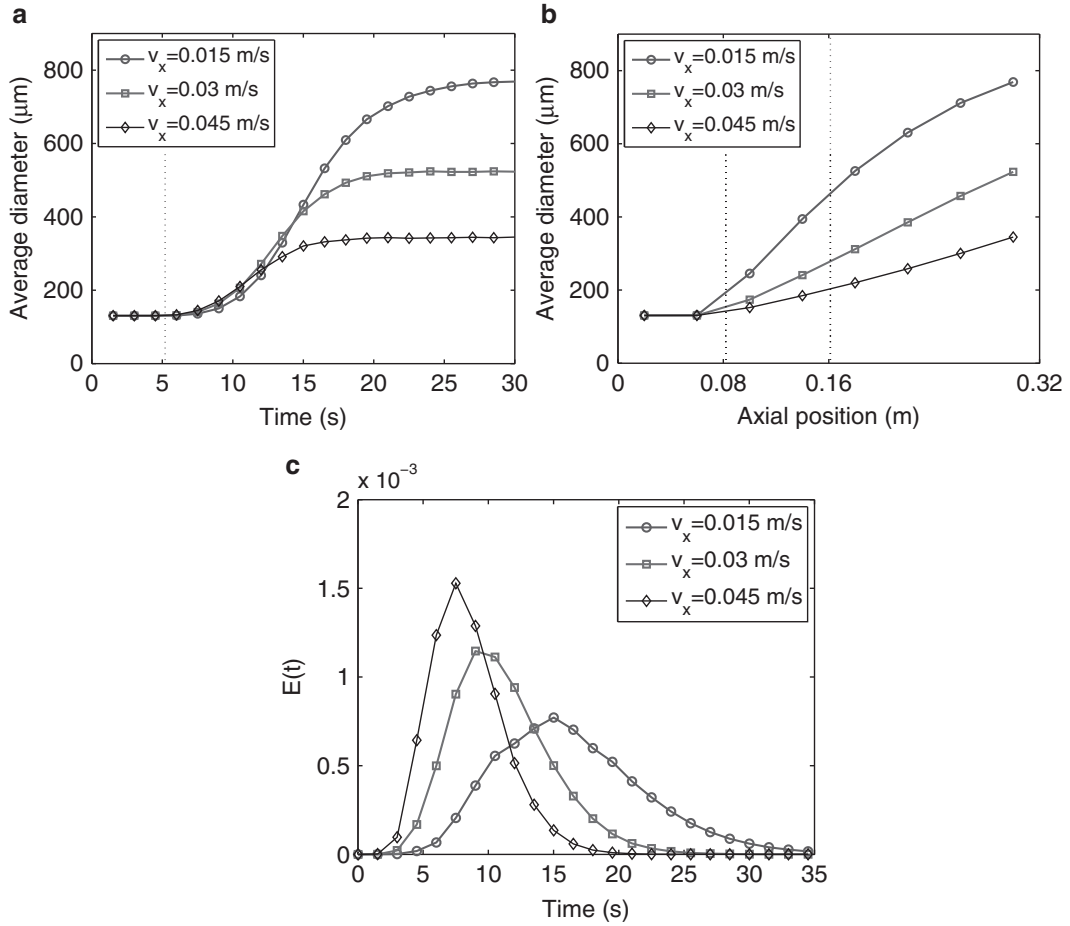


Fig. 9 Average diameter at the outlet vs. time for varying (a) axial velocity, (b) average diameter vs. axial position for varying axial velocities, where vertical lines represent the axial bounds of the spray zone. (c) Residence time distributions for varying axial velocities

screen, while larger fragments are contained and experience additional breakage. In all milling processes, the primary mechanism is particle breakage. Particles are subjected to shear or impact forces, which break larger particles into fragments. The breakage rate, distribution of fragment particles, and screen classification determine the product size distribution. These factors can depend on process parameters, such as impeller speed and screen size, as well as material properties, such as ribbon strength and particle size. PBMs can be employed to understand these effects.

Typically, milling processes have been modeled using 1-D PBMs, accounting for variations in particle size [3, 6, 23, 78]. A general 1-D PBM for milling is presented in Eq. (40), which describes the rate of change in the number of particles of each size class in the system.

$$\frac{\partial F(u, t)}{\partial t} = \mathfrak{R}_{\text{break}}(u, t) = \mathfrak{R}_{\text{break, form}}(u, t) - \mathfrak{R}_{\text{break, dep}}(u, t) \quad (40)$$

Here, $F(u, t)$ represents the number of particles in the system of size u at time t . $\mathfrak{R}_{\text{break}}$ is the breakage term, accounting for the formation of particles due to the breakage of larger particles, $\mathfrak{R}_{\text{break, form}}$, and the depletion of particles as they break into smaller fragments, $\mathfrak{R}_{\text{break, dep}}$. Expressions for the formation and depletion rates are given in Eqs. (41) and (42):

$$\mathfrak{R}_{\text{break, dep}}(u, t) = S(u)F(u, t) \quad (41)$$

$$\mathfrak{R}_{\text{break, form}}(u, t) = \int_u^{\infty} S(v)F(v)b(u, v)dv \quad (42)$$

Here, $S(u)$ is the breakage rate kernel for a particle of size u , and $b(u, v)$ is the fragment distribution, describing the probability that a particle of size u will result in a fragment of size v . While the depletion rate depends only on the number of particles and breakage kernel, the formation rate is more complex. The rate of fragment formation depends on the breakage rates and numbers of particles of all size classes larger than the size class in consideration, resulting in an integral term. Additionally, the breakage distribution function is necessary to describe the sizes of the fragments.

Some studies use a constant rate kernel [78], while various size-dependent rate kernels are also found in the literature [64, 65, 95]. The breakage rate kernel depends on the material properties of the formulation, as well as the process conditions. While these kernels are empirical, a mechanistic breakage kernel for granulation was developed by Ramachandran et al. [73] and can be applied to milling processes. Similarly, various breakage distribution functions have been proposed, including the Hill–Ng distribution [25], a bimodal lognormal distribution [78], and a lognormal distribution [3]. Selection of an appropriate breakage rate kernel and fragment distribution depends on the desired complexity of the model and the ability to describe experimental data.

For a mill operated in batch mode, the mill is treated as a closed system, and any material that passes through the screen is considered a part of the system. The breakage rate $S(u)$ is used to characterize the screen, and small particles are represented with breakage rates of zero as they have passed through the screen and can no longer break. The size cut-off value is often extracted from experimental data [78].

The breakage rate kernel, fragment distribution, and screen model contain parameters that are unknown and must be evaluated

empirically. Parameter estimation has been employed to determine unknown parameters by Reynolds [78], Capece et al. [13], and Barrasso et al. [3].

As a case study, Barrasso et al. [3] developed a 1-D PBM for a continuous conical screen mill, accounting for the effects of impeller speed and screen size. Experimental data was collected from a conical screen mill (Quadro 197-S) using pure microcrystalline cellulose (Avicel PH 200). A full-factorial $2 \times 3 \times 2$ experiment was performed to measure the effects of screen size (3 levels), impeller speed (2 levels), and ribbon density (2 levels) on the product size distribution and mass hold-up.

The PBM incorporated inlet and outlet flow rates, \dot{F}_{in} and \dot{F}_{out} , to represent the feed and product streams of the continuously operated mill, as shown in Eq. (43) [3]:

$$\frac{\partial F(u, t)}{\partial t} = \mathfrak{R}_{\text{break}}(u, t) + \dot{F}_{\text{in}}(u, t) - \dot{F}_{\text{out}}(u, t) \quad (43)$$

Using this approach, $S(u)$ only describes the breakage rate but does not account for the screen. An expression for \dot{F}_{out} was formulated to describe the likelihood that a particle will leave the mill, shown in Eq. (44):

$$\dot{F}_{\text{out}} = (\mathfrak{R}_{\text{break, form}}(u) - \mathfrak{R}_{\text{break, dep}}(u) + \dot{F}_{\text{in}}(u))(1 - f_d(u)), \quad (44)$$

where f_d is a classification function given by Eq. (45) [3]:

$$f_d(u) = \begin{cases} 0 & \text{for } d(u) \leq (1 - \delta)d_{\text{screen}} \\ \frac{d(u) - (1 - \delta)d_{\text{screen}}}{\delta d_{\text{screen}}} & \text{for } (1 - \delta)d_{\text{screen}} \leq d(u) \leq d_{\text{screen}} \\ 1 & \text{for } d(u) > d_{\text{screen}} \end{cases} \quad (45)$$

In this equation, $d(u)$ represents the diameter of a particle in size class u , d_{screen} is the screen aperture, and δd_{screen} is the cut-off size at which particles are large enough to be held up by the screen, assumed to be proportional to the screen size.

An empirical shear rate- and size-dependent breakage kernel was adapted from Pandya and Spielman [64] to account for the effect of impeller speed, v_{imp} on the breakage rate, shown in Eq. (46):

$$S(u) = P_1 v_{\text{imp}} u^{P_2} \quad (46)$$

In this equation, P_1 is a rate coefficient and P_2 describes the size-dependence of the breakage rate. Both parameters must be evaluated experimentally.

Finally, a log-normal fragment size distribution was assumed, given by Eq. (47):

$$b(u, v) = \frac{C(v)}{u\sigma} \exp \left[-\frac{(\log u - \mu(v))^2}{2\sigma^2} \right], \quad (47)$$

where $\mu(v)$ and σ describe the mean and variance of the fragment size distribution formed from a particle of size v , and $C(v)$ is a normalization constant [3]. The mean of the fragment distribution was defined to be proportional to the log of the parent particle size.

Using this data, parameter estimation was performed for each ribbon density to determine five unknown model parameters. For each ribbon density, four of the six experiments were used in parameter estimation. The calibrated model was then used to simulate the remaining two experiments (at the intermediate screen size), and the resulting particle size distributions were compared. The simulated and measured particle size distributions for the low density ribbon showed strong agreement, as shown in Fig. 10 [3]. Once validated, a PBM can be used as a tool to predict the CQAs based on process parameters, demonstrating a model-based approach to QbD.

3 Numerical Techniques to Solve Population Balance Models

The solution of a population balance equation can be obtained using various methods, such as direct discretization, Monte Carlo and the method of moments. Direct discretization is a straightforward approach to obtain an accurate estimate of the particle size distribution, but a disadvantage associated with this methods is the inaccuracy with tracking the moments [41]. Monte Carlo methods are more stochastic in nature and can be used to obtain the solution of multi-component or poly-disperse population balance equation, provided that the probability of dynamic behavior in the system obeys the balance principle for system details, the time step for each successful event can be calculated accurately and all the events occurring in the system are mutually dependant [29, 59]. Various other techniques, such as the method of classes [69], the method of characteristics [28], the method of moments [44, 56], and high resolution algorithms [34] have been used to solve PBMs. Direct discretization techniques, such as the finite difference method, finite element method, and finite volume method, are quite popular for solving PBMs [36, 55]. A more systematic approach known as the hierarchical two tier algorithm was proposed by Immanuel and

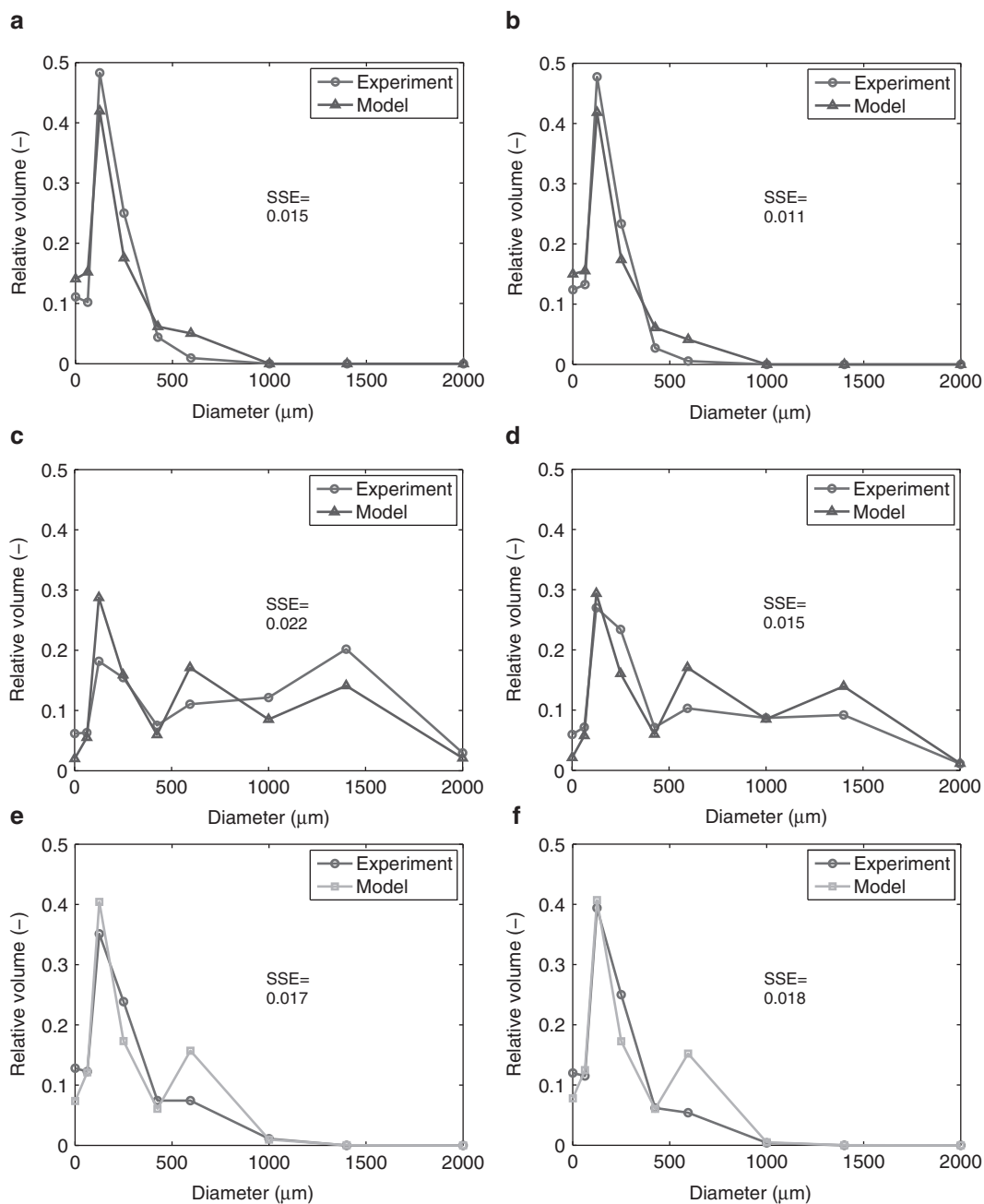


Fig. 10 Experimental and simulated particle size distributions from low density ribbons using (a–d) parameter estimation and (e–f) predictive modeling, by screen aperture and impeller speed [3]. (a) 991 μm , 3350 RPM, (b) 991 μm , 4923 RPM, (c) 3175 μm , 3350 RPM, (d) 3175 μm , 4923 RPM, (e) 1575 μm , 3350 RPM, and (f) 1575 μm , 4923 RPM

Doyle III [36]. The partial differential equation can be discretized (with respect to spatial/internal coordinates) to obtain a set of ODEs (as shown in Eq. (48) for the 3-D PBM for granulation), which can then be solved using a standard Runge Kutta or Euler technique.

$$\begin{aligned}
 & \left. \frac{dF'_{i,j,k}}{dt} + \frac{F'_{i,j,k}}{\Delta s_i} \frac{ds}{dt} \right|_{s_i} - \left. \frac{F'_{i,j,k+1}}{\Delta s_{i+1}} \frac{ds}{dt} \right|_{s_{i+1}} + \left. \frac{F'_{i,j,k}}{\Delta l_j} \frac{dl}{dt} \right|_{l_j} \\
 & - \left. \frac{F'_{i,j,j+1}}{\Delta l_{j+1}} \frac{dl}{dt} \right|_{l_{j+1}} + \left. \frac{F'_{i,j,k}}{\Delta g_k} \frac{dg}{dt} \right|_{g_k} - \left. \frac{F'_{i,j,k+1}}{\Delta g_{k+1}} \frac{dg}{dt} \right|_{g_{k+1}} \\
 & = \mathfrak{R}_{\text{agg}}(s_i, l_j, g_k) + \mathfrak{R}_{\text{break}}(s_i, l_j, g_k)
 \end{aligned} \quad (48)$$

Here $F'_{i,j,k} = \int_{s_i}^{s_{i+1}} \int_{l_j}^{l_{j+1}} \int_{g_k}^{g_{k+1}} F(s, l, g) ds dl dg$, s_i is the value of the solid volume at the upper end of the i th bin along the solid volume axis, l_j is the value of the liquid volume at the upper end of the j th bin along the liquid volume axis, and s_k , l_k , and g_k are the values of the solid, liquid, and gas volume at the upper end of the i th, j th, and k th bins along the solid, liquid, and gas volume axes, respectively. Δs_i , Δl_j and Δg_k are the sizes of the i th, j th and k th bins.

The solution to PBMs is highly computationally expensive. It is thus desirable to develop approaches by which the computational complexity can be alleviated. The discretization of the PBM can be performed using a linear or a nonlinear grid. A linear grid requires a large number of bins to span a certain size range. However a nonlinear grid can span the same range using fewer bins, thus reducing the computational overhead [17]. Various algorithms have been developed to implement a nonlinear grid for discretization [14, 40, 41, 49]. It is most accurate to employ multi-dimensional PBMs to represent the various particulate processes [38]. However, sometimes there are difficulties in solving such system of equations due to the “curse of dimensionality.” It has been pre-established that with an increase in the dimensionality of the PBM, the computation for the aggregation term increases polynomially [67]. The computational expense associated with calculating the aggregation term has been split or redistributed and the overall solution technique has been sped up by parallelizing the code [67, 68].

Another approach for alleviating the computational load for the solution to PBMs is the development of reduced order models. A lower dimensional model was developed by Barrasso and Ramachandran [2] which involved lumping the model in terms of certain independent coordinates in order to reduce the computational expense. The results from the reduced order model suggest a reasonable approximation of the original high dimensional model. As expected, the accuracy of the results reduces as the number of

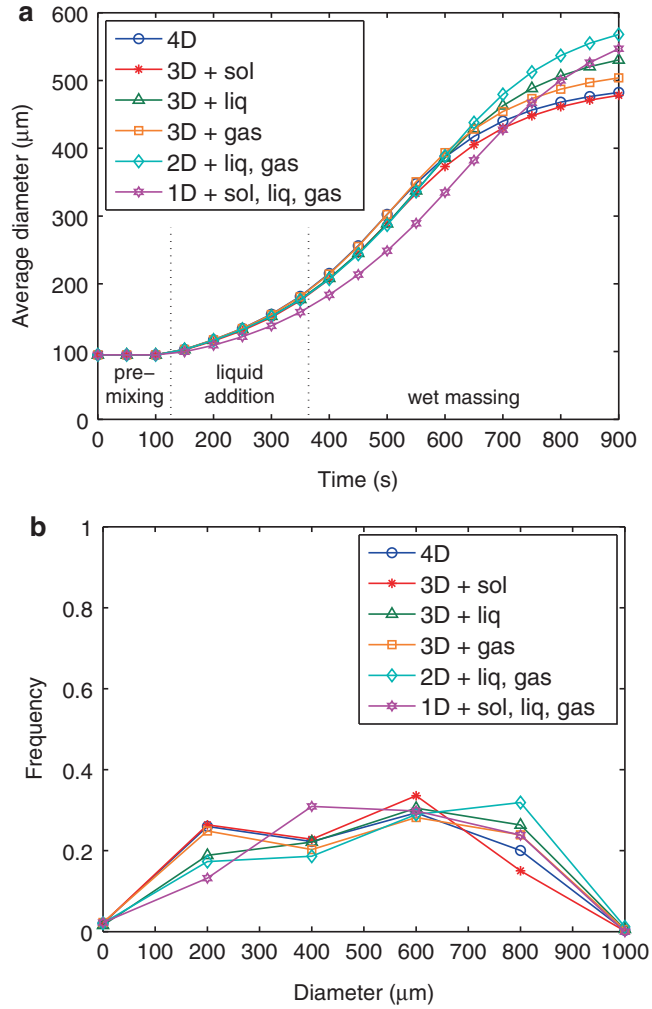


Fig. 11 Comparison of output properties for particle size based on different lumped models. (a) Average diameter over time and (b) normalized particle size distribution at final time

lumped variables is increased (see Fig. 11). It is thus advisable to choose an appropriate framework with a certain extent of lumping which balances the speed and accuracy of the simulations. The ability to discretize a differential equation using a larger number of finer grids reduces the chances of introducing a discretization error (which is a function of the step size for the discretization) into the solution. The appearance of such an instance can be minimized by using a large number of bins for the discretization and also keeping the associated computational time at a reasonable value. For this purpose, the tensor-decomposition approach has been used (implemented in MATLAB by Oseledets et al.) which compresses large volumes of data in the form of a tensor transformation

thus enabling significant savings in the computational time and memory for the simulations [62]. The aggregation term has been calculated as a convolution with the help of fast fourier transforms (FFT). The breakage term and the associated breakage distribution is calculated by separation of variables and reformulating the summation to calculate the equivalent integral terms. The detailed approach for performing the tensor decomposition on the pre-existing high dimensional model has been described in [19].

4 Parameter Estimation

Effective parameter estimation is very crucial for model calibration in order to utilize the mathematical model for predictive purposes. Estimation of empirical parameters requires the need for matching the model outcome with the experimental data. The required experimental data for model calibration might vary for every unit operation. Typically for crystallization processes, the experimental data utilized are the solute concentration in the mother liquor, crystal size [5], and shape. These quantities can be used to fit the model output for calibration purposes. In order to study mixing, the typical data measured in the experiments are the outlet concentration of the powder over time. This information can be utilized to derive various quantities such as RSD and RTD [85]. For studying the agglomeration associated with the mixing process, particle size data can be utilized. In case of granulation processes, the particle size and porosity data are typically considered for parameter estimation purposes [20]. Particle size data also plays a crucial role in the model calibration of milling processes [3].

Parameter estimation is performed by implementing an optimization algorithm that can minimize the mismatch between the model outcome and the experimental data. The objective function ϕ can be written as

$$\phi = (CQA_{\text{simulated}} - CQA_{\text{experimental}})^2 \quad (49)$$

Here, CQA is utilized for the simulated and the experimental results. The CQA varies for each unit operation. The objective function/error can be minimized using various optimization algorithms, such as Nelder–Mead algorithm, various gradient based algorithms, or meta-heuristic techniques (such as genetic algorithm, particle swarm algorithm). With the availability of extensive data, and based on the needs, multiple CQAs can be simultaneously used to fit the model. This can be implemented using a multi-objective optimization algorithm. There are various means by which multiple objective functions can be simultaneously taken into consideration. Using multiple objective functions, there is a

need to obtain the pareto optimal solution. The multiple objective functions can be tackled in various ways—sum/weighted sum of objective functions, min-max method, ε -constraint method. The optimization algorithm efficiently minimizes the error between the simulated and the experimental results thus fitting the model to the system under consideration. The calibrated model can then be utilized for making predictions of the process outcome.

5 Flowsheet Applications of PBM in Pharmaceutical Manufacturing

Detailed process modeling is highly beneficial towards improved process operation for pharmaceutical drug manufacturing. The formulation of a PBM requires an in-depth understanding of the process physics and associated risks. Thus, development of a first principles-based PBM leads to compliance with the guidelines of QbD as proposed by the FDA. Using effective parameter estimation techniques to calibrate the model (as discussed in the previous sections) contributes to the predictive ability of the PBM framework. PBMs can also be utilized for performing control and optimization of various particulate processes. Some of the works presenting a control strategy for improved process operation include [54, 72, 93].

In recent years, a large thrust is observed, pushing the drug manufacturing mode from batch to continuous. This would not only involve modernizing the overall process with more sophisticated equipment/control strategies but also the need for modifying the mathematical models for improved process understanding [45]. Some benefits of adopting the continuous manufacturing route include the use of the same equipment for the production of variable quantities of drug, thus minimizing the need for scale-up studies and reducing the time-to-market. This also enables the entire setup to fit in a much smaller space. Also, in a continuous setting, the human factor is significantly reduced through automation of operation and thus overheads incurred due to labor can be minimized. Drug products can be continuously manufactured using one of the three primary routes, as selected based on the material being handled. These routes are, namely, direct compaction, roller compaction, and wet granulation [8]. Figure 12 shows the continuous mode for running the upstream and downstream processes for drug manufacturing. Within this flowsheet, various unit operations can be addressed using a PBM are crystallization, granulation, milling, mixing, and coating. In the previous sections a brief description has been provided on the extension of the PBMs for batch operation to continuous operation. Boukouvala et al. [9, 10] have performed detailed studies on simulating and optimizing the downstream pharmaceutical drug manufacturing in continuous mode. Sen et al. [84, 87] have conducted studies on

developing and analyzing the upstream purification process in the continuous mode.

The flowsheet modeling approach provides a more accurate representation of the continuous manufacturing mode due its consideration of the unit operations in an integrated framework. All the unit operations within the flowsheet framework are not represented using population balances, however several complex unit operations are described using population balance models. The properties of the solid/mixture change at the exit of every unit operation is accounted into the flowsheet model and can successfully describe/explain the evolution of powder properties over the continuous manufacturing framework.

Figure 12 also shows the critical quality attributes (CQA) that are of concern at the exit of each unit operation. It can be seen that

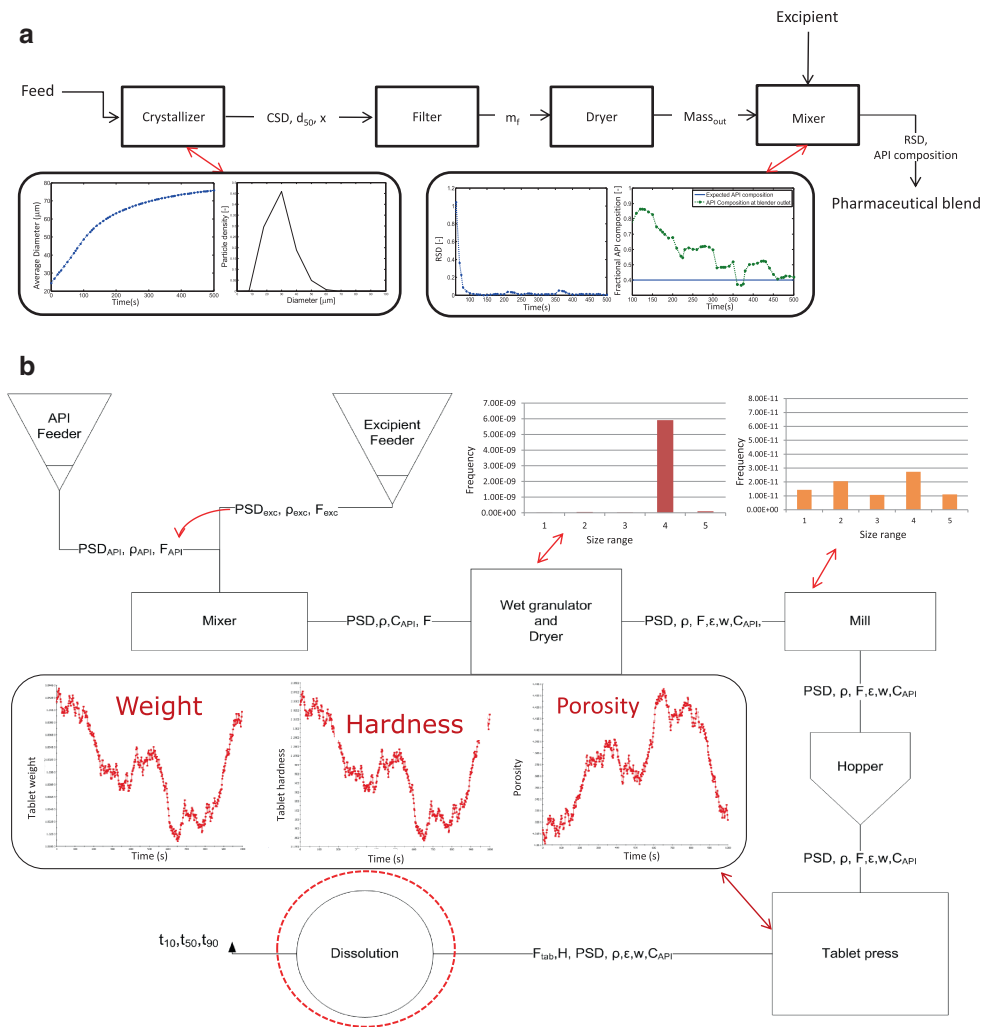


Fig. 12 Flowsheet modeling of continuous downstream pharmaceutical drug manufacturing. (a) Upstream tablet manufacturing and (b) downstream tablet manufacturing using wet granulation route

using the corresponding model, such exit properties can be tracked. Boukouvala et al. [9] have also performed a sensitivity analysis for the flowsheet models and have studied how noise gets propagated through the multiple unit operations present in the flowsheet. This enables the identification of noise propagation through the continuous operation and can provide the upper bounds to the extent of upset that would keep the system within the acceptable range of operation. Sen et al. [87] performed optimization studies coupled with a multiscale model on the upstream pharmaceutical manufacturing process in order to maximize the efficiency of the overall operation. The crucial parameters affecting each unit operation were identified, which were then fed into the optimization algorithm with the flexibility to be manipulated such that the overall flowsheet could be optimized. Various PBMs were also a part of the flowsheet, which enabled to alleviate the inefficiencies associated with the continuous operation mode. With the development of sophisticated and mechanistic models that can effectively capture the trends in continuous manufacturing operation, the overall understanding of the continuous operation can be enriched and the operation of the process can be improved.

6 Conclusions

There exists a significant amount of inefficient operation in the pharmaceutical industry which suggests the need for a model-based system approach in order to alleviate the operation of the process and reduce wastes. Using a model based approach, the number of experimental trials can be significantly reduced, thus accelerating the profits made by the industry. Population balance models are highly useful for modeling the processes relevant to the pharmaceutical industry, due to its ability to effectively capture the dynamics of a discrete particulate process. Population balance models can be used to describe the process involving solid handling and can be further used to make effective predictions. Parameter estimation techniques enable the quantification of the empirical constants within the model thus extending the utility of the model to make predictions. A brief overview of the parameter estimation techniques is presented in this chapter and provides guidance on the applicability of this framework for predictive purposes. This aligns very closely with the principles of QbD/Process Analytical Tools (PAT) that has been recently proposed by the US FDA.

In order to effectively use this framework for improving the process operation, development of numerical techniques for solution of PBMs is essential. Various numerical techniques have surfaced over the past decade that enable effective solution to PBMs. Some of those techniques have also been briefly discussed in Sect. 3. The “curse of dimensionality” can be overcome using

reduced order models as discussed above. Since pharmaceutical drug manufacturing mostly involves the handling of powder and other particulate matter (such as crystals), employing PBMs for modeling such processes is an effective approach. With the advent of a paradigm shift in the mode of process operation for drug manufacturing, the operation of the continuous manufacturing process requires the study of the integrated process using a flow-sheet modeling approach. Several unit operations within the flow-sheet model are represented using PBMs. From the discussions presented above, it can be clearly inferred that PBMs play a vital role in modeling pharmaceutical processes, primarily due to the inherent discrete nature of PBMs.

References

1. Abbas A, Romagnoli JA (2007) Multiscale modeling, simulation and validation of batch cooling crystallization. *Sep Purif Technol* 53 (2):153–163
2. Barrasso D, Ramachandran R (2012) A comparison of model order reduction techniques for a four-dimensional population balance model describing multi-component wet granulation processes. *Chem Eng Sci* 80:380–392
3. Barrasso D, Oka S, Muliadi A, Litster JD, Wassgren C, Ramachandran R (2013) Population balance model validation and prediction of cqs for continuous milling processes: toward QbD in pharmaceutical drug product manufacturing. *J Pharm Innov* 8:147–162
4. Barrasso D, Walia S, Ramachandran R (2013) Multi-component population balance modeling of continuous granulation processes: a parametric study and comparison with experimental trends. *Powder Technol* 241:85–97
5. Besenhard MO, Chaudhury A, Vetter T, Ramachandran R, Khinast J (2015) Evaluation of parameter estimation methods for crystallization processes modeled via population balance equations. *Chem Eng Res Des* 94: 275–289
6. Bilgili E, Scarlett B (2005) Population balance modeling of non-linear effects in milling processes. *Powder Technol* 153(1):59–71
7. Borissova A (2009) General systems modeling of multi-phase batch crystallization from solution. *Chem Eng Process Process Intensif* 48 (1):268–278
8. Boukouvala F, Ramachandran R, Muzzio FJ, Ierapetritou M (2011) Computer-aided design of an integrated pharmaceutical process. *Comput Aided Chem Eng* 6:100–105
9. Boukouvala F, Niotis V, Ramachandran R, Muzzio FJ, Ierapetritou MG (2012) An integrated approach for dynamic flowsheet modeling and sensitivity analysis of a continuous tablet manufacturing process. *Comput Chem Eng* 42:30–47
10. Boukouvala F, Chaudhury A, Sen M, Zhou R, Mioduszewski L, Ierapetritou M, Ramachandran R (2013) Computer-aided flowsheet simulation of a pharmaceutical tablet manufacturing process incorporating wet granulation. *J Pharm Innov* 8(1):11–27
11. Braatz RD (2002) Advanced control of crystallization processes. *Annu Rev Control* 26 (1):87–99
12. Cameron I, Wang F, Immanuel C, Stepanek F (2005) Process systems modelling and applications in granulation: a review. *Chem Eng Sci* 60 (14):3723–3750
13. Capece M, Bilgili E, Dave R (2011) Identification of the breakage rate and distribution parameters in a non-linear population balance model for batch milling. *Powder Technol* 208 (1):195–204
14. Chakraborty J, Kumar S (2007) A new framework for solution of multidimensional population balance equations. *Chem Eng Sci* 62 (15):4112–4125
15. Chaudhury A, Ramachandran R (2013) Integrated population balance model development and validation of a granulation process. *Part Sci Technol* 31(4):407–418
16. Chaudhury A, Tabora JE, Murugesan S, Remy B, Ramachandran R (2011) Application of a 2-d population balance model to a pharmaceutical crystallization process. In: *Proceedings of 2011 AIChE annual meeting, Minneapolis, October 2011*
17. Chaudhury A, Kapadia A, Prakash AV, Barrasso D, Ramachandran R (2013) An extended cell-average technique for a multi-dimensional

- population balance of granulation describing aggregation and breakage. *Adv Powder Technol* 24(6):962–971
18. Chaudhury A, Niziolek A, Ramachandran R (2013) Multi-dimensional mechanistic modeling of fluid bed granulation processes: an integrated approach. *Adv Powder Technol* 24(1):113–131
 19. Chaudhury A, Oseledets IV, Ramachandran R (2013) A computationally efficient technique for the solution of multi-dimensional population balance models of granulation via tensor decomposition. *Comput Chem Eng* 61:234–244
 20. Chaudhury A, Barrasso D, Pandey P, Wu H, Ramachandran R (2014) Population balance model development, validation, and prediction of cqas of a high-shear wet granulation process: towards qbd in drug product pharmaceutical manufacturing. *J Pharm Innov* 9(1):53–64
 21. Chaudhury A, Wu H, Khan M, Ramachandran R (2014) A mechanistic population balance model for granulation processes: effect of process and formulation parameters. *Chem Eng Sci* 107:76–92
 22. Costa CBB, Maciel MRW, Filho RM (2007) Considerations on the crystallization modeling: population balance solution. *Comput Chem Eng* 31(3):206–218
 23. Datta A, Rajamani RK (2002) A direct approach of modeling batch grinding in ball mills using population balance principles and impact energy distribution. *Int J Miner Process* 64(4):181–200
 24. Denis C, Hemati M, Chulia D, Lanne JY, Buisson B, Daste G, Elbaz F (2003) A model of surface renewal with application to the coating of pharmaceutical tablets in rotary drums. *Powder Technol* 130(1–3):174–180
 25. Diemer RB Jr, Spahr DE, Olson JH, Magan RV (2005) Interpretation of size reduction data via moment models. *Powder Technol* 156(2–3):83–94
 26. Ennis BJ, Tardos G, Pfeffer R (1991) A microlevel-based characterization of granulation phenomena. *Powder Technol* 65(1–3):257–272
 27. Fazli NA, Samad A, Singh R, Sin G, Gernaey KV, Gani R (2011) A generic multi-dimensional model-based system for batch cooling crystallization processes. *Comput Chem Eng* 35(5):828–843
 28. Févotte F, Févotte G (2010) A method of characteristics for solving population balance equations (pbe) describing the adsorption of impurities during crystallization processes. *Chem Eng Sci* 65(10):3191–3198
 29. Fichtom KA, Weinberg WH (1991) Theoretical foundations of dynamical monte carlo simulations. *J Chem Phys* 95(2):1090–1096
 30. Freireich B, Li J, Litster J, Wassgren C (2011) Incorporating particle flow information from discrete element simulations in population balance models of mixer-coaters. *Chem Eng Sci* 66(16):3592–3604
 31. Gernaey KV, Gani R (2010) A model-based systems approach to pharmaceutical product-process design and analysis. *Chem Eng Sci* 65:5757–5769
 32. Gerogiorgis DI, Barton PI (2009) Steady-state optimization of a continuous pharmaceutical process. In: 10th International symposium on process systems engineering: Part A, computer aided chemical engineering, vol 27, pp 927–932
 33. Goldhirsch I (2008) Introduction to granular temperature. *Powder Technol* 182:130–136
 34. Gunawan R, Fusman I, Braatz RD (2004) High resolution algorithms for multidimensional population balance equations. *AIChE J* 50(11):2738–2749
 35. Hounslow MJ, Ryall RL, Marshall VR (1988) A discretized population balance for nucleation, growth, and aggregation. *AIChE J* 34(11):1821–1832
 36. Immanuel CD, Doyle III FJ (2003) Computationally efficient solution of population balance models incorporating nucleation, growth and coagulation: application to emulsion polymerization. *Chem Eng Sci* 58(16):3681–3698
 37. Immanuel CD, Doyle III FJ (2005) Solution technique for a multi-dimensional population balance model describing granulation processes. *Powder Technol* 156(2–3):213–225
 38. Iveson SM (2002) Limitations of one-dimensional population balance models of wet granulation processes. *Powder Technol* 124:219–229
 39. Klatt KU, Marquardt W (2009) Perspectives of process systems engineering-personal views from academia and industry. *Comput Chem Eng* 33:536–550
 40. Kumar J, Peglow M, Warnecke G, Heinrich S, Mörl L (2006) Improved accuracy and convergence of discretized population balance for aggregation: the cell average technique. *Chem Eng Sci* 61(10):3327–3342
 41. Kumar S, Ramkrishna D (1996) On the solution of population balance equations by discretization-i. A fixed pivot technique. *Chem Eng Sci* 51(8):1311–1332
 42. Kumar R, Wassgren C (2013) Angular circulation speed of tablets in a vibratory tablet

- coating pan. *AAPS PharmSciTech* 14(1): 339–351
43. Laloue N, Couenne F, Gorrec YL, Kohl M, Tanguy D, Tayakout-Fayolle M (2007) Dynamic modeling of a batch crystallization process: a stochastic approach for agglomeration and attrition process. *Chem Eng Sci* 62 (23):6604–6614
44. Lee K (1983) Change of particle size distribution during brownian coagulation. *J Colloid Interface Sci* 92(2):315–325
45. Leuenberger H (2001) New trends in the production of pharmaceutical granules: batch versus continuous processing. *Eur J Pharm Biopharm* 52:289–298
46. Li J, Freireich B, Wassgren C, Litster JD (2012) A general compartment-based population balance model for particle coating and layered granulation. *AIChE J* 58(5): 1397–1408
47. Lindenberg C, Krättli M, Cornet J, Mazzotti M (2009) Design and optimization of a combined cooling/antisolvent crystallization process. *Cryst Growth Des* 9(2):1124–1136
48. Litster J, Ennis B (2004) *The science and engineering of granulation processes*. Kluwer Academic Publishers, Dordrecht
49. Litster JD, Smit DJ, Hounslow MJ (1995) Adjustable discretized population balance for growth and aggregation. *AIChE J* 41(3): 591–603
50. Liu LX, Litster JD (2002) Population balance modelling of granulation with a physically based coalescence kernel. *Chem Eng Sci* 57 (12):2183–2191
51. Liu LX, Litster JD, Iveson SM, Ennis BJ (2000) Coalescence of deformable granules in wet granulation processes. *AIChE J* 46(3): 529–539
52. Liu L, Robinson D, Addai-Mensah J (2012) Population balance based modelling of nickel laterite agglomeration behaviour. *Powder Technol* 223:92–97
53. Long C, Gantt J, Gatzke E (2005) Batch granulation control using a simplified population balance and nonlinear model predictive control. In: *Proceedings of the 2005 American control conference*, 2005, vol 2, pp 949–954
54. Ma DL, Tafti DK, Braatz RD (2002) Optimal control and simulation of multidimensional crystallization processes. *Comput Chem Eng* 26(7–8):1103–1116
55. Marchal P, David R, Klein J, Villiermaux J (1988) Crystallization and precipitation engineering—i. An efficient method for solving population balance in crystallization with agglomeration. *Chem Eng Sci* 43(1):59–67
56. Marchisio DL, Soos M, Sefcik J, Morbidelli M, Barresi AA, Baldi G (2006) Effect of fluid dynamics on particle size distribution in particulate processes. *Chem Eng Technol* 29 (2):191–199
57. Maronga S, Wnukowski P (1997) Establishing temperature and humidity profiles in fluidized bed particulate coating. *Powder Technol* 94 (2):181–185
58. Maronga S, Wnukowski P (1997) Modelling of the three-domain fluidized-bed particulate coating process. *Chem Eng Sci* 52 (17):2915–2925
59. Marshall CL Jr, Rajniak P, Matsoukas T (2011) Numerical simulations of two-component granulation: comparison of three methods. *Chem Eng Res Des* 89(5):545–552
60. Miki H, Terashima T, Asakuma Y, Maeda K, Fukui K (2005) Inclusion of mother liquor inside kdp crystals in a continuous msmpr crystallizer. *Sep Purif Technol* 43(1):71–76
61. Nakamura H, Abe E, Yamada N (1998) Coating mass distributions of seed particles in a tumbling fluidized bed coater part ii. A monte carlo simulation of particle coating. *Powder Technol* 99(2):140–146
62. Oseledets IV, Tyrtshnikov EE (2009) Breaking the curse of dimensionality, or how to use SVD in many dimensions. *SIAM J Sci Comput* 31(5):3744–3759
63. Pandey P, Tao J, Chaudhury A, Ramachandran R, Gao JZ, Bindra DS (2013) A combined experimental and modeling approach to study the effects of high-shear wet granulation process parameters on granule characteristics. *Pharm Dev Technol* 18(1):210–224
64. Pandya J, Spielman L (1983) Floc breakage in agitated suspensions: effect of agitation rate. *Chem Eng Sci* 38(12):1983–1992
65. Pinto MA, Immanuel CD, Doyle III FJ (2007) A feasible solution technique for higher-dimensional population balance models. *Comput Chem Eng* 31(10):1242–1256
66. Portillo PM, Muzzio FJ, Ierapetritou MG (2008) Using compartment modeling to investigate mixing behavior of a continuous mixer. *J Pharm Innov* 3:161–174
67. Prakash AV, Chaudhury A, Barrasso D, Ramachandran R (2013) Simulation of population balance model-based particulate processes via parallel and distributed computing. *Chem Eng Res Des* 91(7):1259–1271
68. Prakash AV, Chaudhury A, Ramachandran R (2013) Parallel simulation of population balance model-based particulate processes using multicore CPUs and GPUs. *Model Simul Eng*. doi:10.1155/2013/475478

69. Puel F, Févotte G, Klein J (2003) Simulation and analysis of industrial crystallization processes through multidimensional population balance equations. Part 1: a resolution algorithm based on the method of classes. *Chem Eng Sci* 58(16):3715–3727
70. Qamar S, Galan K, Elsner MP, Hussain I, Seidel-Morgenstern A (2013) Theoretical investigation of simultaneous continuous preferential crystallization in a coupled mode. *Chem Eng Sci* 98:25–39
71. Ragnarsson G, Johansson MO (1988) Coated drug cores in multiple unit preparations influence of particle size. *Drug Dev Ind Pharm* 14 (15–17):2285–2297
72. Ramachandran R, Chaudhury A (2012) Model-based design and control of a continuous drum granulation process. *Chem Eng Res Des* 90(8):1063–1073
73. Ramachandran R, Immanuel CD, Stepanek F, Litster JD, Doyle III FJ (2009) A mechanistic model for breakage in population balances of granulation: theoretical kernel development and experimental validation. *Chem Eng Res Des* 87(4):598–614
74. Ramkrishna D (2000) Population balances. Academic, San Diego
75. Reklaitis GV, Khinast J, Muzzio F (2010) Pharmaceutical engineering science - new approaches to pharmaceutical development and manufacturing. *Chem Eng Sci* 65:iv–vii
76. Remy B (2010) Granular flow, segregation and agglomeration in bladed mixers. PhD thesis, Rutgers, The State University of New Jersey
77. Remy B, Khinast J, Glasser B (2009) Discrete element simulation of free flowing grains in a four-bladed mixer. *AIChE J* 55:2035–2058
78. Reynolds GK (2010) Modelling of pharmaceutical granule size reduction in a conical screen mill. *Chem Eng J* 164(2–3):383–392
79. Ronsse F, Pieters J, Dewettinck K (2007) Combined population balance and thermodynamic modelling of the batch top-spray fluidised bed coating process. Part I—model development and validation. *J Food Eng* 78 (1):296–307
80. Salman AD, Hounslow MJ, Seville JPK (2007) Granulation. Elsevier, Amsterdam
81. Sastry KV (1975) Similarity size distribution of agglomerates during their growth by coalescence in granulation or green pelletization. *Int J Miner Process* 2(2):187–203
82. Sen M, Ramachandran R (2013) A multi-dimensional population balance model approach to continuous powder mixing processes. *Adv Powder Technol* 24:51–59
83. Sen M, Singh R, Vanarase A, John J, Ramachandran R (2012) Multi-dimensional population balance modeling and experimental validation of continuous powder mixing processes. *Chem Eng Sci* 80:349–360
84. Sen M, Chaudhury A, Singh R, John J, Ramachandran R (2013) Multi-scale flowsheet simulation of an integrated continuous purification-downstream pharmaceutical manufacturing process. *Int J Pharm* 445(1–2):29–38
85. Sen M, Chaudhury A, Singh R, Ramachandran R (2014) Two-dimensional population balance model development and validation of pharmaceutical crystallization processes. *American Journal of Modern Chemical Engineering* 1: 13–29
86. Sen M, Dubey A, Singh R, Ramachandran R (2013) Mathematical development and comparison of a hybrid pbm-dem description of a continuous powder mixing process. *J Powder Technol*. [dx.doi.org/10.1155/2013/843784](https://doi.org/10.1155/2013/843784)
87. Sen M, Rogers A, Singh R, Chaudhury A, John J, Ierapetritou MG, Ramachandran R (2013) Flowsheet optimization of an integrated continuous purification-processing pharmaceutical manufacturing operation. *Chem Eng Sci* 102:56–66
88. Sherony DF (1981) A model of surface renewal with application to fluid bed coating of particles. *Chem Eng Sci* 36(5):845–848
89. Stephanopoulos G, Reklaitis GV (2011) Process systems engineering: from solvay to modern bio- and nanotechnology: a history of development, successes and prospects for the future. *Chem Eng Sci* 66(19):4272–4306
90. Tan HS, Goldschmidt MJV, Boerefijn R, Hounslow MJ, Salman AD, Kuipers JAM (2004) Building population balance model for fluidized bed melt granulation: lessons from kinetic theory of granular flow. *Powder Technol* 30:103–109
91. Vanarase AU (2011) Design modeling and real time monitoring of continuous powder mixing processes. PhD thesis, Rutgers, The State University of New Jersey
92. Vanarase A, Muzzio F (2011) Effect of operating conditions and design parameters in a continuous powder mixer. *Powder Technol* 208(1):26–36
93. Vanderroost M, Ronsse F, Dewettinck K, Pieters J (2008) Population balance model for quality control of coating processes in fluidised beds. In: Proceedings of XVI international conference on bioencapsulation, p 23–1
94. Verkoefen D, Pouw GA, Meesters GMH, Scarlett B (2002) Population balances for

- particulate processes—a volume approach. *Chem Eng Sci* 57(12):2287–2303
95. Vogel L, Peukert W (2003) Breakage behaviour of different materials—construction of a mastercurve for the breakage probability. *Powder Technol* 129(1–3):101–110
96. Wang F, Ge X, Balliu N, Cameron I (2006) Optimal control and operation of drum granulation processes. *Chem Eng Sci* 61(1):257–267
97. Wauters P (2001) Modelling and mechanisms of granulation. PhD thesis, Delft University of Technology, Delft
98. Wnukowski P, Setterwall F (1989) The coating of particles in a fluidized bed (residence time distribution in a system of two coupled perfect mixers). *Chem Eng Sci* 44(3):493–505

Process Simulation and Data Modeling in Solid Oral
Drug Development and Manufacture

Ierapetritou, M.G.; Ramachandran, R. (Eds.)

2016, X, 393 p. 131 illus., 96 illus. in color., Hardcover

ISBN: 978-1-4939-2995-5

A product of Humana Press